EFFECT OF FALLEN POSIDONIA OCEANICA SEAGRASS LEAVES ON WAVE ENERGY AT SANDY BEACHES

by

Ogan Sevim

B.S., Civil Engineering, Dokuz Eylül University, 2001

M.S., Civil Engineering, Boğaziçi University, 2005

Submitted to the Institute for Graduate Studies in
Science and Engineering in partial fulfillment of
the requirements for the degree of
Doctor of Philosophy

Graduate Program in Civil Engineering

Boğaziçi University

2024

ACKNOWLEDGEMENTS

Some encounters cause significant changes in a person's life. Meeting Prof. Emre Otay was one such encounter. I decided to embark on this challenging academic journey without any hesitation under his guidance. I am deeply grateful to Prof. Emre Otay for his support, and patience with me throughout this extraordinary scientific adventure. I will always proudly state that I was his student.

I would like to thank to Thesis Committee Members and Thesis Jury Members, Prof. Özer Çinicioğlu, Prof. Servet Karasu, Prof. Nadim Copty, Prof Serdar Soyöz and Asist. Prof. Burak Ali Çiçek for their contributions during thesis progress and defence.

I would like to thank to Mr. Onur Akagündüz for his supports during preparation and execution of field tests. Also special thanks to Mr. Muhammed Aslan, my doctoral classmate, for his support both in field tests and during model studies.

I would like to thank to my colleagues in Zetas Zemin Teknolojisi A.Ş. for their patience while I was sparing time for PhD Studies and they have to compensate my absence. I am also grateful to Soletanche Bachy and Municipality of Alanya for their support for the execution of the field tests.

I would like to express my deepest gratitude to my mother Hülya, my father Ahmet, and my brother Burak, who have brought me to where I am today, always supported every decision I made, and believed in me. Finally, I would like to extend my special thanks to my family, my dear wife Merve, and my sons Ahmet Safa and Ogan Efe. Every hour I spent on this work is a debt I owe to you. I will strive to make up for it in the rest of our lives. I always motivated myself by thinking that I would be a good example for my sons. I hope they feel the positive impact of this in their lives.

ABSTRACT

EFFECT OF FALLEN POSIDONIA OCEANICA SEAGRASS LEAVES ON WAVE ENERGY AT SANDY BEACHES

Posidonia Oceanica (PO) is an endemic marine vegetation for the Mediterranean Sea. In an experimental study, conducted in the Eastern Mediterranean, natural dead PO leaves are measured to reduce incident wave heights impacting the beach. Transmission coefficient (K_t) was found to vary between 0.73-0.94 which is equivalent to a wave height decay of 6-27%. The results show that the free-floating dead PO leaves in their natural environment dissipate incoming wave energy and have a capacity to protect the beach against erosion. Further analysis in separate frequency bands show that short waves (with periods less than 4.4 s) are more sensitive to PO leaves in terms of energy dissipation. The transmission coefficient for short waves as calculated using the high frequency part of the wave spectrum, delivered a maximum transmission coefficient of 0.5 corresponding to 50% wave height decay due to PO leaves.2D model was established with an open-source software and calibration of the model was done with data without PO leaves. Vegetation parameters are incorporated to the calibrated model and wave decays are calculated by changing drag coefficients and second calibration of the model is done with vegetation with mean-root-square error of 4 mm which is 2% of the observed wave heights. Free parameter selected for calibration was drag coefficient (CD) and kept fixed throughout the analysis since the Reynold's number was in the range of 4-9.10^3 . Finally, an empirical, wave length depended wave decay formula is derived.

ÖZET

POSİDONİA OCEANİCA DENİZ ÇAYIRLARININ ÖLÜ YAPRAKLARININ KUM KIYILARDAKİ DALGA ENERJİSİNE ETKİLERİ

Posidonia Oceanica (PO) Akdeniz'e özgü bir deniz bitkisidir. Doğu Akdenizde gerçekleştirilen deneysel çalışma ile, doğal ölü PO yapraklarının kıyıyı etklileyen deniz dalgalarının yüksekliklerini etkilediği ölçülmüştür. Dalga yayılma katsayılarının (K_t) 0.73 ile 0.94 arasında değiştiği, bununda dalga boyu sönümlenmesinin %6-27 arasında gerçekleştiği gözlemlenmiştir. Deney sonuçları, denizde serbest dolaşan ölü PO yaprakların doğal ortamlarında, kıyı erozyonuna neden olan dalga enerjisine karşı koruma kapasitesi olduğunu göstermektedir. Farklı frekans bantlarda yapılan ileri analizlerde PO yapraklarının kısa dalgalara karşı (peryodu 4.4 sn'den düşük dalgalar) enerji sönümlemesine karşı daha hassas olduğunu göstermektedir. Dalga Spektrumunun yüksek frekans kısmında yapılan hesaplamalarda, en düşük yayılma katsayınının 0.5 olduğu ve bununda %50 dalga sönümlenmesine tekabul etmektedir. İki boyutlu dalga transformasyon programı kullanılarak iki boyutlu bir model oluşturuldu ve modelin kalibrasyonu, PO yaprakları olmadan alınan verilerle yapıldı. Kalibre edilmiş modele bitki parametreleri eklenerek, sürükleme ve katsayıları değiştirilerek dalga yüksekliklerindeki sönümlemeler hesaplandı. Sürükleme katsayısı ölçülen değerlerle ile model değerleri arasındaki kök ortalama kare hatası 4 mm yani ölçülen değerlerin %2 sine tekabül edene kadar devam ettirildi. İkinci kalibrasyonda serbest parametre olan sürükleme katsayısı 0.55 olarak bulundu. Reynolds sayısı 4-9.103 aralığında hesaplandığı için sürükleme katsayısı analiz boyunca sabit tutuldu. Son olarak, dalga boyuna bağlı ampirik bir dalga sönüm formülü türetilmiştir.

TABLE OF CONTENTS

LIST OF FIGURES

LIST OF TABLES

LIST OF SYMBOLS

A	Cross-section area of plant
a	Wave amplitude
a_0	Initial wave amplitude
b	Spacing between plants
c	Celerity of wave
ca	Cauchy number
C_b	Bottom friction coefficient
C_D	Drag coefficient
$\tilde{C_D}$	Bulk drag coefficient
C_g	Group velocity of waves
C_{g0}	Initial group velocity
D	Energy dissipation
D_{tot}	Total energy dissipation
d_p	Diameter of the plant
E	Energy
E_0	Initial energy
F	Energy flux
F	Fourier transform
F^{-1}	Inverse fourier transform
F_D	Drag force
g	Acceleration of gravity
h	Water depth
H	Wave height
H_0	Initial wave height
H_{m0}	Significant wave height
$H_{m0-shallow}$	Significant wave height at shallow location
$H_{m0-deeep}$	Significant wave height at deep location
H_{rms}	Root mean square of wave height

K	Dissipation coefficient
k	Wave number
k_i	Exponential decay coefficient
K_p	Dynamic response factor
K_r	Refraction coefficient
k_r	Real part of complex wave number
K_s	Shoaling coefficient
K_t	Transmission coefficient
K_v	Damping coefficient
L	Wavelength
m_0	Zeroth moment of spectral density function
m_n	Nth moment of spectral density function
N	Wave action
N	Number of plant per unit area
$p(H)$	Probability density function of wave heights
p	Pressure
p_D	Dynamic pressure
Re	Reynold's Number
s	Height of the plant
$S(f)$	Spectral density function
$S_{ds,b}$	Energy dissipation by bottom friction
$S_{ds,veg}$	Energy dissipation by vegetation
St	Station
S_{tot}	Total energy sink and source
T_{m02}	Mean wave period
T_p	Peak period
T'	Dimensionless period
t	Time
$X(t)$	Seawater surface elevation function
X'	Relative test field length
X	Horizontal length of the test field

X	Horizontal coordinate normal to shoreline
u	Horizontal orbital velocity
z	Vertical coordinate
α	Leave concentration parameter
$\tilde{\beta}$	Decay coefficient
β	Leave concentration related constant
δ	Leave concentration related constant
η	Sea level elevation
ν	Dynamic viscosity
ρ	Seawater density
σ	Angular velocity of wave

LIST OF ACRONYMS/ABBREVIATIONS

1D	One Dimensional
2D	Two Dimensional
ADCP	Acoustic Doppler Current Profiler
AST	Acoustic Surface Tracking
CTD	Conductivity Temperature Depth
FT	Fourier Transform
Hz	Hertz
HP	Horsepower
IFT	Inverse Fourier Transform
KC	Kauleguen Carpenter Number
MHz	Mega Hertz
NBS	Nature Based Solution
PG1	Pressure Gauge 1
PG2	Pressure Gauge 2
PO	Posidonia Oceanica
PVC	Poly Vinyl Chloride

1. INTRODUCTION

Coastal areas are the transition regions between mainland and oceans and since the beginning of human history, coastal regions are in the interest of human beings owing to its benefits such as productive lands which was emerged trough sediments brought by rivers, easy access to other regions through maritime facilities and source of food from the sea. According to United Nation's reports 40% of human population lives within the coastal region, where the coastal region is defined as 100 km inland from the shoreline. Presently, economic reasons such as tourism, and recreation are the main reason for the people settle in those regions [1]. Therefore, sandy beaches in coastal zones are under anthropologic stress on top environmental stresses such as sea level rise, drought in terrestrial zone, and extreme storm events which may be attributed to climate change. Anthropologic stresses can be uncontrolled building of sea structures such as groins and seawalls, uncontrolled sediment mining, sediment deficit due to dams and run-off river power plants. Coastal erosion is the main result of those anthropogenic and environmental stresses which is expected to be a growing problem globally and particularly in the Mediterranean Coasts. Depending on the location, economic and environmental impacts will be higher on beaches with tourism revenue. Sandy beaches provide habitat for many species including sea turtles, shellfish, starfish etc which are also threatened by erosion.

Regardless of whether it is environmental or anthropogenic, coastal erosion on sandy beaches is driven by longshore and cross-shore sediment transport without sufficient sand source in the shoreline system. Longshore sediment transport along a beach is proportional to the 2.5th power of the breaking wave height [2] whereas the wave energy is proportional to the square of the wave height. Wave induced bottom shear stress causes suspension of sediments which are then transported by means of wave induced currents. On cross-shore direction sediment transport would be either in onshore direction which results with accretion or in offshore direction which results in erosion. Direction of sediment is defined by Dean's (1973) fall time model. In this

model fall time is defined as average distance of sediment in water column from the bottom, divided by the falling velocity of sand grains. According to Dean (1973) if fall time is less than half the wave period, particles tend to transport onshore direction which results with accretion and vice versa if the fall time is greater than half wave period it results erosion [3]. Although sand size dominates the fall time, average distance of the sediment is proportional to the wave breaker height since most of the sediment resuspension occurs at the breaker point. Therefore, we can conclude that waves and wave induced currents are the main factor for beach erosion both in cross-shore and longshore direction.

Although there is no general study that quantifies the overall erosion around the Turkish coasts, there are many studies on the local scale. For example, Yılmaz *et al.* (2015) studied the erosion problem in Silifke, Mersin, Türkiye and measured 100 m sand recession in 40 years at the barrier which is separating Paradeniz Lagoon with the Mediterranean Sea [4]. In another study, Yuksek et al (1995) studied the coastal erosion in the Eastern Black Sea region of Turkey for about 450 km of coastline and proposed different erosion protection methods for 23 sites out of 27 where investigation carried out [5]. However, the problem is country wide and many news articles about erosion problem for different locations can be found in local media. In Figure 1.1 image of a coastal erosion which destroyed the beach Eastern Coasts of Alanya, Türkiye is presented.

Figure 1.1. Image of coastal erosion in east coast of Alanya, Turkey (Photo credit: Author).

Many methods are applied to protect the beaches against erosion in the engineering practice. Methods may be classified into two categories: hard measures and soft measures. The term "hard" refers to hard structures such as groins, revetments, seawall and, emergent and submerged breakwaters. Although hard measures may prevent coastal erosion locally, there are many adverse effects of such structures on the macro scale of the coastal region. For instance, once a groin is constructed in an erosive beach, while sand accumulates on the upstream side of the littoral drift, erosion will take at the downstream side of the groin. These phenomena will lead the necessity of construction additional groins in the downstream which will lead a "snowball effect" as it was experienced in many coasts of Türkiye such as, Karasu, Edremit and Bafra, where additional beach protection construction tenders are floated by the Minister of Environment, Urbanization and Climate Change several time. A similar case of uncontrolled groin construction can be seen in the Mediterranean Turkler region between Alanya and Antalya in Figure 1.2. Between 2013 and 2017 number of groins increased from 2 to 12 and continues erosion in the downstream side of is visible from the image (downstream is the right side of image). There are many secondary effects of hard measures which is beyond the scope of this study. Soft measures can be considered sand nourishment, sand trapping and, geotubes.

Figure 1.2. Historical changes of the erosion protection in Türkler Region, Alanya, Türkiye [6].

In addition to hard and soft solutions, nature-based solutions (NBS) are becoming interest of stakeholders owing to its environmental and economic benefits. Sea bottom vegetation is one of the examples of the NBS against coastal erosion. Sea bottom vegetation may supplement or even replace conventional erosion protection techniques. Many studies have been carried out about impact of sea vegetation on wave properties and sediment dynamics in last decades. Details of these studies will be provided in the preceding sections.

In this study, focus is given to the wave energy dissipation capacity of the sunken or floating leaves of dead seagrass , Posidonia Oceanica (PO), in the nearshore (Figure 1.3). Along the Mediterranean coast, large meadows of PO are observed where new leaves can bloom all year around. In autumn, the dead leaves fall off the rhizomes and accumulate inside the meadows. Autumn and winter storms drive the fallen PO leaves away from the meadows to other ecosystems [7]. Most of the time they end up washing ashore where they form up natural banquettes at the beach if not artificially removed or degrade biologically. Therefore, large amount of dead PO leaves moves back and forth in the nearshore depending on seasonal coastal dynamics.

Figure 1.3. Posidonia oceanica dead leaves in the breaking and surf zone (Photo credit: Author).

Our hypothesis is since dead PO leaves involves in nearshore dynamics, they must interact with water particles and since they are transported back and forth, work done by the waves (and or currents) must lead a dissipation on the wave energy which results wave decay. In Figure 1.4 an image of dead PO leave cluster within the nearshore and breaking zone can be seen in two frames just before the breaking and during breaking. The cluster of dead PO leaves can be seen in the marked circle, and it is obvious that while the wave ray is breaking in the right and left side of the cluster, wave height is reduced, and breaking is retarded within the cluster zone.

Figure 1.4. Photo of wave breaking within a dead PO leave cluster. Fugla Beach, Alanya 2022 (Photo credit: Author).

Although the fate and transportation of dead PO leaves are not well known, by observation we can state that they are washed ashore and return to sea until they

are deposited to sheltered zone in coastal areas. In some cases, PO leaves remains between beach face and the nearshore back and forth all year around in steep beaches. For example, in Damlatas Beach in Alanya as shown in Figure 1.5 dead leaves can be seen as a black strip in nearshore and in the absence of sheltered area they remain in the nearshore unless they are removed by hoteliers from the beach when they are temporarily washed ashore. Therefore, we hypothesise that PO leaves contribute to coastal hydrodynamics by reducing the wave height therefore wave energy, which improves the beach built-up.

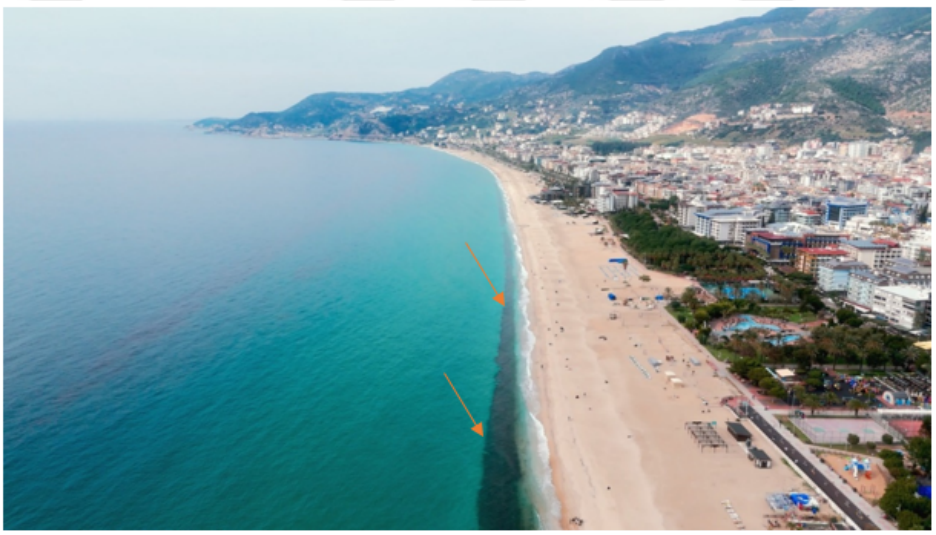

Figure 1.5. Damlatas Beach in Alanya, Dead PO Leaves Deposited in Nearshore (Black Shade as Strip, Photo Credit: Author).

If our hypothesis is true, this may have an impact on beach erosion measures since in most of the touristic regions, dead leaves are removed from the beach as soon as they washed ashore due to recreational reasons. Techniques to deploy dead leaves in the beach defence may be developed which may reduce the cost of construction of hard structures. Beside the economic impact, such techniques might be environmentally beneficial as well. Dead leaves are source of nutrition to many other species and returning dead leaves back to ocean will enrich the marine habitat.

Dead leaves have density between 800-1020 kg/m^3 [8]. However due to adhered fine particles the density of the bulk dead leaves might be much higher than afore mentioned values. Depending on the adhered particle concentration dead leaves might be floating, suspending, or sunk. Notwithstanding the position of the dead leaves in the sea, they are subjected to traction of water particles as they move in orbital motion as they move shoreward. Our hypothesis is during the traction between water particles dead leaves may not follow the exact motion of the water particles due to cluster structure of the leaves and relative motion occurs. The resulting drag between water particle and PO leaves reduce the orbital velocity of the water particle and in this way wave celerity reduces and wave height decays.

To prove our hypothesis, a field test is performed by using natural dead PO leaves in semi-controlled manner in nearshore with shallow water waves and in a zone with mild slope (1/30). To verify the findings in the field tests, a customized 1D ray model developed based on small amplitude wave theory. Also, a two-dimensional (2D) model is setup to incorporate the vegetation impact on wave transformation. Our finding indicates dead PO leave decay the waves between 6-27% and the free-floating dead PO leaves in their natural environment dissipate incoming wave energy and have a capacity to protect the beach against erosion. Further analysis in separate frequency bands show that short period waves (with periods less than 4.4 s) are more sensitive to PO leaves in terms of energy dissipation. Whereas long period waves (with periods more than 6.7 s) are not sensitive. The transmission coefficient for short period waves as calculated using the high frequency part of the wave spectrum, delivered a maximum transmission coefficient of 0.5 corresponding to 50% wave height decay due to PO leaves. It is concluded that the PO leaves operate like a low pass filter on incoming waves and dissipate incident short waves more efficiently. Therefore, in closed seas with shorter fetch and wave periods, the PO leaves may work as efficient as a floating breakwater which have similar transmission coefficients. The maximum transmission coefficient of 0.5 as it was found in the study corresponds to wave energy dissipation of 75 % as the wave energy is proportional to the square of the wave height.

Similarly, the wave induced beach erosion may drop by 82 % because of the higher exponent in the breaker height to sediment transport relation.

Wave decay ratios given above does not contain any shoaling impact. In no vegetation case both 1D ray and 2D models calculates wave transmission coefficients higher than 1 i.e., between 1.1-1.4. Considering transmission coefficients based on shoaled wave heights, the decay ratio is much greater than values given above. Details of the findings will be presented in the preceding sections.

The outline of this thesis is as follows: In Chapter 2, a brief literature survey on sea vegetation will be provided. Seasonal cycle of PO leaves is presented and theoretical models developed for wave damping capacity of sea vegetation are provided. A brief on the laboratory and field experiments on the live meadows is summarized. In Chapter 3, methodology used in the thesis is presented. Methodology is inclusive of field measurement, 1D and 2D modelling of the measurement area with and without PO leaves. In Chapter 4, field measurement and data analysis are presented in detail including properties of the measurement devices, bathymetric conditions, and data processing methods. Chapter 5 includes models developed for verification of the field tests and calibration of the existing models developed in literature. In Chapter 6, results of 1D ray model and 2D model are compared with the field test findings and comprehensive analysis is presented. Chapter 7 contains the conclusion of the study and recommendation of author for further studies.

2. LITERATURE SURVEY

2.1. Posidonia Oceanica

Posidonia Oceanica (PO) is an endemic marine vegetation for the Mediterranean Sea which covers 50.000 km^2 of area which is 25% of the entire basin shallower than the 40 m [9,10]. It is an important Carbon sink (Named as "Blue Carbon" owing to colour of the ocean) and absorbs almost same amount of carbon as terrestrial forests. According to Lavery *et al.*, Posidonia Oceanica has carbon storage, up to 40–410 kg/m^2 [11].

European Environmental Agency, classified PO meadows are as "priority habitat" (Directive 92/43/CEE) due to its importance in the Mediterranean ecosystem and recent recession in meadows among the European coasts. They have rhizomes and strip type leaves with length between 80-100 cm and which may go up 150 cm. The width of the leaves is between 8-11 mm with thickness of around 1 mm. In one rhizome, there are 4-5 leaves whereas in meadow number of rhizomes can be in the range of 400-900 per m^2 which leads 2000-4500 leaves per m^2 [7,12].

In a meadow, new leaves form all the year around with a lifespan of 5- 8 months. Once new leaves form the dead leaves drops off and transported within nearshore by the waves or elsewhere with current. In Figure 2.1 image of a meadow presented which is taken in April 2023 at Fugla Beach, between Antalya and Alanya in Türkiye. In spring new leaves are the most and therefore meadows are greenish. During summer as the leaves dies the meadow gets brownish.

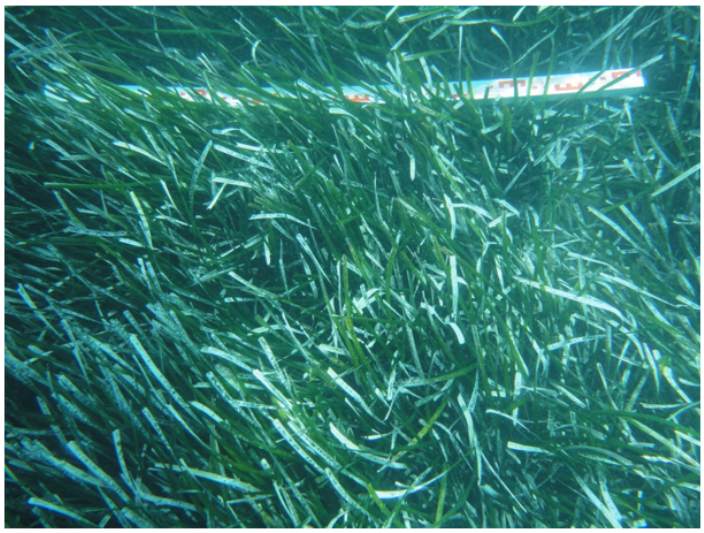

Figure 2.1. Image of posidonia oceanica meadow in Fugla Beach, Alanya, Türkiye (Spring, 2023, Photo credit: Author).

Once rhizomes of PO dies, together with other organic remains within the meadows, create kind of a reef which is termed as "matte" (Figure 2.2). Growth of meadow is in the range of one meter per 100 years and can go up to one meter below the water surface level [11]. PO matte may form a kind of berm structure within the sea bottom which may trap the sediment within the nearshore or act as submerged breakwater and improves the beach.

Figure 2.2. Posidonia oceanica "matte" in Fugla Beach, Alanya, Türkiye (Spring, 2023).

2.2. Theoretical Models of Wave Dissipation by Sea Vegetation

Before presenting existing theoretical models on wave dissipation of vegetation, it is worthwhile to mention that in literature focus is given mostly on the live plants fixed at the sea bottom. One of the earliest studies on the wave decay by sea vegetation is done by Price *et al.* (1968) which they modelled the artificial seaweed and investigate the impact on beach built-up [13]. They propose simple wave decay model assuming water has different viscosity within the meadow and viscosity of the bottom layer dominates the wave decay. A wave decay coefficient is defined as

$$K = (\frac{2 * \nu}{\sigma})^{\frac{1}{2}} \frac{k^2}{2kh + sinh(2kh)}, \tag{2.1}$$

where K is the dissipation coefficient, ν is the dynamic viscosity of the water within the meadow, σ is the wave frequency, k is the wave number and h is the water depth and the sea level variation is given by

$$\eta(x) = a_0 e^{(} - Kx) cos(kx - \sigma t), \tag{2.2}$$

where η is the sea level elevation, a_0 is the initial amplitude, x is horizontal distance. In their study Price *et al.* (1968) also made laboratory tests in a wave flume and used plastic mimics of seaweeds and showed that vegetation decays the waves by 4% and increase the shoreward sand transport 3 times [14].

During subsequent years, theoretical models are developed to predict wave attenuation induced by sea vegetation. Dalrymple *et al.* (1984) generalized The National Academy of Sciences procedure for damping of waves by trees and developed mathematical model for wave attenuation which is based on the drag work done by the vegetable blades. They modelled the vegetation as rigid cylinders and ignored the relative motion between the blades and the water particles. A Morrison-type drag force is vertically integrated along the stem height to calculate the drag work and the energy dissipation per unit meadow area [15]. Derivations starts with conservation of energy which is the change rate of energy flux is direct correlated with energy dissipation as follow

$$\frac{\partial F}{\partial x} = -D, \tag{2.3}$$

where F is the energy flux, x is the horizontal coordinate positive towards onshore and, D is the dissipation of wave energy. Energy flux is defined as

$$F = EC_g, \tag{2.4}$$

where, € is the wave energy per unit area and C_g is the group velocity of the wave train and wave energy and group velocity are defined as

$$E = \frac{1}{2}\rho g a^2, \tag{2.5}$$

$$C_g = nc, \tag{2.6}$$

where ρ is the density of sea water, g is the acceleration of gravity, a is the wave amplitude, c is the celerity n and c is defined as follows

$$n = \frac{1}{2}(\frac{1+2kh}{sinh2kh}), \tag{2.7}$$

$$c = \sqrt{\frac{g}{k}}tanhkh, \tag{2.8}$$

Assuming horizontal bottom and without any dissipation other than the vegetation, right hand side of the Equation (2.3) would be the work done by the drag forces encountered to the vegetation

$$D = F_D u, \tag{2.9}$$

where F_D is the drag force and u is the horizontal component of the wave orbital velocity. From small amplitude wave theory, we know that u is calculated with below formula

$$u = \frac{agk}{\sigma}(\frac{cosh(k(h+z)}{cosh(kh)})cos(kx - \sigma t), \tag{2.10}$$

where z is the vertical coordinate with origin at the mean sea level, a is the amplitude of the wave and F_D can be calculated with below formula

$$F_D = \frac{1}{2}\rho C_D A N u^2, \tag{2.11}$$

where ρ is the density of the water, C_D is the drag coefficient, A is cross section area of the plant and, N is the number of stems per unit area of the meadow. If we plug Equation (2.10) and Equation (2.11) into Equation (2.9), we will get dissipation for unit area as follows

$$D = \frac{1}{2}\rho C_D A N(\frac{agk}{\sigma}(\frac{cosh(k(h+z)}{cosh(kh)})cos(kx - \sigma t))^3. \tag{2.12}$$

If we integrate Equation (2.12) over the length of the vegetation in vertical direction where the height of the vegetation from the bottom of the sea is defined as s

$$D = \int_{-h}^{s-h} \frac{1}{2}\rho C_D A N(\frac{agk}{\sigma}(\frac{cosh(k(h+z))}{cosh(kh)})cos(kx-t))^3)dz, \tag{2.13}$$

$$D = 2a^3\rho\frac{C_D}{3\pi}\frac{d_p}{k}\frac{(sinh^3(ks)+3sinh(ks))}{2cosh^3(kh)}(\frac{gk}{\sigma})^3(\frac{1}{b^2}), \tag{2.14}$$

where b is the spacing between vegetation stems and, d_p is the diameter of width of individual stems x and t are horizontal coordinate positive to onshore direction and time respectively and s is the height of plant. If we plug Equation (2.14) to Equation (2.3), we get

$$\frac{\partial F}{\partial x}\frac{1}{2} = \rho g C_g \frac{da^2}{dx} = -Ba^3, \tag{2.15}$$

where B can be formulated as follows

$$B = 2\rho\frac{C_D}{3\pi}\frac{d_p}{k}\frac{(sinh^3(ks)+3sinh(ks))}{2cosh^3(kh)}(\frac{gk}{\sigma})^3(\frac{1}{b^2}). \tag{2.16}$$

Solution to Equation (2.15) can be written in below form

$$\frac{a}{a_0} = \frac{1}{(1+\alpha x)}, \tag{2.17}$$

where α is the decay coefficient and given with below formulation

$$\alpha = (\frac{2C_D}{3\pi})(\frac{d_p}{b})(\frac{a_0}{b})(sinh^3(ks)+3sinh(ks))[\frac{4k}{3sinh(kh)(sinh(2kh)+2kh)}], \tag{2.18}$$

Kobayashi *et al.* (1993) [16] also used similar approach of Dalrymple *et al.* (1984) by including the drag forces within momentum equations and assuming that waves will be decayed exponentially while travelling through vegetation wave height variation would be as per below formulation

$$H(x) = H_0 e^{(-k_i x)}, \tag{2.19}$$

where $H(x)$ is the wave height at any point on the vegetation, H_0 is the incident wave height before the wave entering vegetation zone and, k_i is the exponential decay coefficient which formulation is given as below

$$k_i = \varepsilon \frac{2k_r + sinh(2k_r s)}{2k_r h + sinh(2k_r h)}, \tag{2.20}$$

where k_r is the real part of the complex wave number and ε is given with below formulation

$$\varepsilon = \frac{1}{9\pi} C_D A N H_0 \frac{sinh(3k_r s) + 9sinh(k_r s)}{2k_r s + sinh(2k_r s) sinh(k_r h)}, \tag{2.21}$$

Mendez and Losada (2004), extended Dalrymple *et al.* (1984) derivation and derived wave dissipation by vegetation in sloping beach [17]. For sloping bottom, they found the wave height variation along the vegetation field as

$$(x) = H_0 K_v K_s, \tag{2.22}$$

where K_v and K_s are damping and shoaling coefficients respectively. K_v is given with below formulation

$$K_v = \frac{1}{1 + 2A_1/mH_0(K_s - 1)}, \tag{2.23}$$

In this formulation m is the bottom slope and A_1 is constant and function of drag coefficient, C_D. In their study, Mendez and Losada (2004) also derived the wave transformation model for random waves where the probability of the wave height distribution follows unmodified Rayleigh distribution. Accordingly, probability density function, $p(H)$, of the wave height with respect to root-mean-square of the wave heights can be written as follows:

$$p(H) = \frac{2H}{H_r ms^2} e^{-(\frac{H}{H_r ms})^2}, \tag{2.24}$$

where H_{rms} is the root-mean-square of the wave heights which is given with below formulation

$$H_{rms}^2 = H^2 p(H) dH, \tag{2.25}$$

if energy flux balance equation can be written in terms of H_{rms} and same procedure with Dalrymple *et al.* (1983) applied we end up below decay formulation for random waves

$$H_{rms} = \frac{H_{(rms,o)}}{(1 + \beta \tilde{x}}, \tag{2.26}$$

where $\tilde{\beta}$ is the decay co-efficient for random waves and calculated with below formulation

$$\tilde{\beta} = \frac{1}{(3)} (\tilde{C_D}) b_\nu N H_{rms} k \frac{sinh^3(ks) + 3sinh(ks)}{(sinh(2kh) + 2kh) sinhkh}, \tag{2.27}$$

The main drawback of above formulations is that vegetation is modelled as rigid cylinders. However, in nature, in most cases, sea vegetation are not rigid cylinders, and they move as the water columns moves back and forth while the wave passes. Therefore, dissipation values calculated with above formulation would be much higher than actual dissipation in nature. On the other hand, both models are assuming that sea bottom is flat and quantity of the plant does not vary with the horizontal distance. It should be noted that quantity of the blades is a function of time and periodic annually as explained in Chapter 2.1

2.3. Laboratory Tests Performed to Measure the Wave Decay by Vegetation

As of today, there is no single widely applied theoretical model to calculate wave decay by vegetation and it may be challenging to develop one.

There are many studies performed in wave flumes to verify wave decay models and calibrate α value in Equation (2.18). As α is function of C_D, drag co-efficient, and all other terms in the equation is known wave flume test results are used to estimate the drag coefficient. On the other hand, using drag coefficient of single stem might be

misleading because of shading effects within the meadow. In summary list of drawbacks on the existing models can be listed as below:

- Models assumes plants are rigid and cylinder.
- They do not consider shading effects.
- Relative velocity between plant and water particles are not considered. Horizontal velocity of the particle is used and correlation between dissipation and horizontal velocity is a cubic function and omitting relative velocity may exaggerate the dissipation.
- Model assumes constant plant parameters such as plant diameter, length, and stem density. However, in nature they are changing by seasons. Temporal changes are annually periodic.

In literature the most common approach to eliminate above listed drawbacks is to define a "bulk drag co-efficient". Based on flume test results, authors correlated bulk drag coefficient with dimensionless parameters such as; Reynold's Number (Re) [18-20,21], Cauchy Number (Ca) [22], or Kauleguen Carpenter Number (KC) [21,23]. Another approach was to use a "effective blade length" that will represent the blades as rigid cylinder [22]. Bradley and Houser (2009) suggests to use Reynold's number as drag co-efficient relation and they claim that KC does not represent the drag co-efficient whereas Mendez and Losada (61) suggested to correlate the bulk drag co-efficient with KC number with a 76% correlation [20,17]. Henry *et al.* (2015) summarized most of the literature and formulations between drag co-efficient and dimensionless parameters and suggested Cauchy Number correlation with the effective blade length [24]. Peruzzo *et al.* (2018) studied the wave attenuation and calculated the drag co-efficient with both KC and Re numbers. While stating that both KC and Re are suitable to estimate the drag co-efficient, they were not able to state which of the drag formulation works better and suggested further study in this area [21].

Formulations of the drag co-efficient, regardless of the dimensionless parameter, contains calibration parameters to be correlated flume test results. On the other hand,

main drawbacks in the flume tests are the similarity problem while mimicking the vegetation and the scale effects. Polyethylene, poly vinyl chloride (PVC), or similar material is used to mimic the flexible vegetation [25]. In some cases, dowels, or wood is used to represent rigid vegetation [26,27]. In very rare case Fonseca and Calahan (1992) and Hendricks *et al.* (2008) had used live vegetation in flume tests which might be very difficult in present due to environmental restrictions [28,29] . Koftis *et al.* (2013) and Manca *et al.* (2012) performed large scale (100 m long) flume tests to minimize the scaling effects [18,30]. It should be noted here that there are studies to identify the relative velocity between plant and water particles. However, applicability of those studies to nature is arguable.

Based on the flume test results done in the past, wave attenuation due to vegetation varies between 4% to 90% of the incident wave height. Chastel *et al.* (2020), used 22 m long artificial vegetated section in their flume and they measured 67.5% wave height reduction [14]. Perruzzo *et al.* (2018) showed that in emergent case of vegetation, up to 90 % of wave height reduction can be observed whereas it is less than 50% in case of submerged vegetation [21]. Elginoz *et al.* (2011) used nickel-chrome made stripe wire to model Posidonia oceanica leaves which is 20 times more rigid than real plants, and the wave height reduction they observed was between 5-22 % depending on the variables they have used in their flume tests [31]. On top of scale effects, large differences in the flume test results are mainly due to variables used during tests such as stem density (number of leaves per m^2) and length, submergence ratio of the vegetation, incoming wave height and period, mimic rigidity etc.

Vegetation type is also important differentiating factor in the capacity of wave height reduction. Fonseca and Calahan (1992) worked on four different types of seagrasses (i.e. Halodule wrightii, S.Filiforme, T. testudinum, and Zostera marina) in a wave flume of 6 m with changing leaf length, water depth, wave type and stem density. Measurement in wave height reduction done, after passing of waves through 1 m of seagrasses. The results indicate that depending on the vegetation type wave height reduction varies in different loading scenarios. Although in average 40 % of reduction

is observed in wave height reduction, for instance, Halodule wrightii showed largest wave height reduction with thinnest leaf thickness. On the other hand, Zostera marina has the broader leaves and showed lowest wave height reduction [28].

One of the rare field tests was done by Bradley and Houser (2007), along the Northern edge of Santa Rosa Island in northwest Florida where the sea bed is covered mainly with Thalassia testudinum seagrasses and, they measured an average significant wave height reduction of 30% after passing 39 m of seagrass meadow[20]. In another study, Zhang *et al.* (2020) made field measurements in north coast of Hangzhou Bay at Jinshan District in Shanghai City, China where the basin is covered with Spartina alterniflora marshes. During four different surge conditions (storm and tide) with varying water depths, Authors measured the wave data and calculated the wave height changes between two measuring station with 10 m. Significant wave height reduction was between 9-23% during measurement stating that lower attenuation measured during higher water depths and higher attenuation measured with higher incident wave heights [32].

2.4. Knowledge Gap in Literature

Almost all existing literature focus to the vegetation which are fixed to the sea bottom via root and classified as per their rigidity, stem density per unit area, length, width, or diameter, emergent or submergent (in case of submergent, submergence ratio or depth). Except few fields test [20,32] most of those tests were performed using flume and mimic of vegetation which would never represent actual conditions in nature. In addition, vegetation parameters which were investigated in flume tests, on contrary, in nature dynamic throughout the year depending on its metabolism. Posidonia Oceanica seagrasses, which has similar life cycle of the those in the terrestrial zones (i.e., they do photosynthesis, they flower and defoliate) stem density is the lowest during winter period [33] when the sea is in most energetic state. However, once they defoliate, tons of dead leaves transported within the sea until they are deposited to the shoreline or degraded within the sea. Therefore, the aim of present study is to investigate wave

attenuation capacity of the defoliated Posidonia Oceanica leaves. Dead leaves can be suspended or sunk at sea bottom depending on their density which varies between 800-1020 kg/m^3 [8]. Although they may contribute to wave attenuation in different forms or stages i.e., while they are in the meadow or after they leave the meadow, our interest is in the phase while the leaves are being transported in the nearshore towards the beach at low energetic coasts.

In addition to experimental studies, theoretical and numerical models are also focused on the vegetation fixed to bottom with rigid and flexible stems as briefly explained in Chapter 2.2. Based on the literature above, it is worthwhile to investigate the impact of dead leaves in their natural environment on wave energy. According to the knowledge of the Author, this subject has not been studied in the past.

3. METHODOLOGY

To prove our hypothesis, below listed methodologies are followed:

- A field measurement was done to measure the decay while the wave passes dead PO leave cluster.
- Two dimensional and one-dimensional custom-made models were developed to analyse the field measurement results.
- An empirical formulation for the wave decay capacity of dead PO leaves based on the field and model results.

3.1. Field Test

To validate our hypothesis, it is essential to understand how incident waves are transformed from deep water to shallow water as they pass above or through a cluster of dead PO leaves. A field test scheme is planned to quantify wave height decay due to PO leaves and calculate the associated energy dissipation. The primary challenge for such measurements is that PO leaves are free-floating, making it difficult to deploy measurement devices at their exact locations in a large environment. In sheltered areas where the sea is less energetic, it is possible to find dead PO leaves, but this environment does not allow for measuring the impact above certain wave heights. Consequently, we have decided to conduct the tests in a "semi-controlled" manner by transporting the PO leaves to a selected location and depositing them in the sea where we intend to measure the wave heights.

As shown section and plan view of the test field in Figure 3.1 and Figure 3.2 respectively, acoustic doppler current profiler (ADCP) measurement device was planned to be deployed in offshore at a sufficient depth that wave parameters with not be effected from shoaling or other hydrodynamic impacts. Two another measurement devices planned to be located just before the PO leaves cluster and after the cluster in the

onshore direction respectively. This arrangement would allow us, to record the wave properties such as wave height, mean period and peak period before entering and, after leaving PO leave zone. Pressure gauge at the offshore side of the PO leave zone was deployed to analyse the shoaling and bed friction effects on wave heights which would be used in the model setup in the next step.

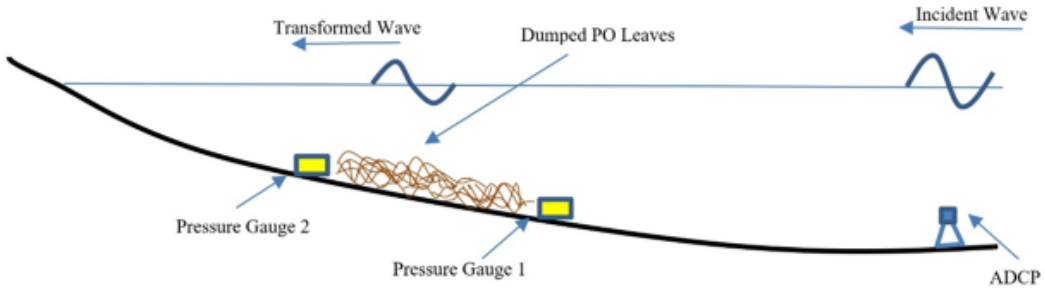

Figure 3.1. Typical section of planned test field.

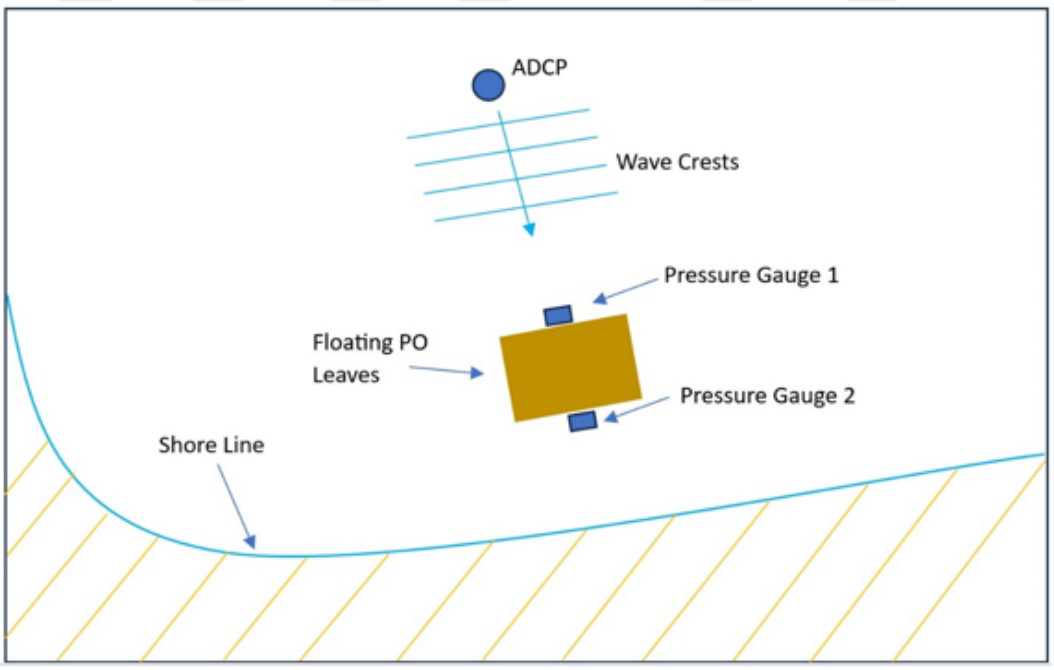

Figure 3.2. Plan view of the planned test field.

Once the devices are located it was planned to release the dead PO leaves in between two pressure gauges we expect three different data as listed below:

- Incident wave properties from ADCP.
- Shallow water wave properties shoaled and decayed by bed friction.
- Shallow water wave properties shoaled and decayed by bed friction and dead PO leaves.

Since the distance between the two pressure gauges is relatively short and the depth variance is minimal, we expect a reduced impact from shoaling and bed friction. Consequently, we anticipate accurately measuring the effect of PO leaves on the wave properties.

3.2. Model Establishment

One dimensional (1D) custom made, and two-dimensional (2D) model is required for further analysis of the results due to complexity of the field tests. Purpose of the models are decomposing wave height reduction due to dissipation by PO leaves, bed friction and wave height increase due to shoaling from the measured water surface elevation data by using existing wave dissipation models. In the analysis, other hydrodynamic impacts such as wave-wave interaction, reflection were neglected. Only bed friction and shoaling are considered.

In 2D model, boundaries and grids were selected according to the locations of the measurement devices. Data collected from ADCP was processed and they were used as the boundary value for both 1D and 2D models. As pressure gauge which is in the offshore side of the field does not affect from the PO leaves, initial calibration was done with the data of this gauge. Once calibration done, for the impact of PO leaves a free parameter of C_D was used as calibration parameter. Other parameters such as number of stems and height of the dead PO leaves within the sea was selected approximate values on trial-and-error basis based on the notes hold during the test and other means such as drone images. More detailed information about the model and results will be provided in Chapter 5.

3.3. Empirical Formulation

At final stage of this thesis and empirical formulation is derived for the wave decay depending on the PO leave concentration, length in the cross-shore direction and incident wave parameter which will be based on the measurement and calibrated models. Shallow water waves approximation is used in the analytical part of the formulation and details are presented in Chapter 6.

4. MEASUREMENT METHOD AND SITE SETUP

4.1. Study Area

The field experiments are conducted at Fugla Bay, a headland beach on the Mediterranean Coast of Turkey located between two touristic cities, Antalya and Alanya as shown in Figure 4.1. The bay has a 1.7 km long sandy beach facing towards the South-West. The area is rich with Posidonia Oceanica (PO) meadows as 40% of the seabed is covered with PO reefs and bedrock outcrop. Rest of the seabed is sandy bottom with a median grain size (d_{50}) of 0.25 mm and with an average slope of 1/30.

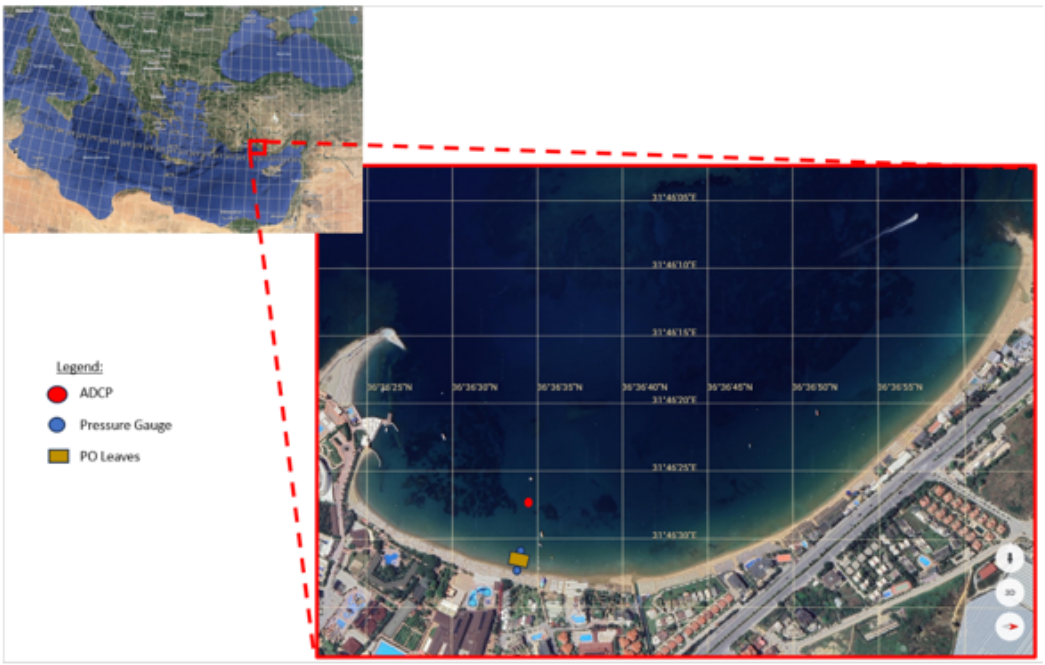

Figure 4.1. Site location and measurement device locations.

Field measurements are conducted in April 2023, a time of year when PO leaves are washed ashore. Although defoliation starts as early as in autumn, it normally takes a few storms until all the leaves are accumulated at the shore.

4.2. Site Bathymetry

Prior to the gauge installation, bathymetric measurements are conducted at the test site. Bottom slope is measured as 1/30. Bathymetric contours of the bay and the bottom profile along the test site are shown in Figure 4.2 and Figure 4.3 respectively.

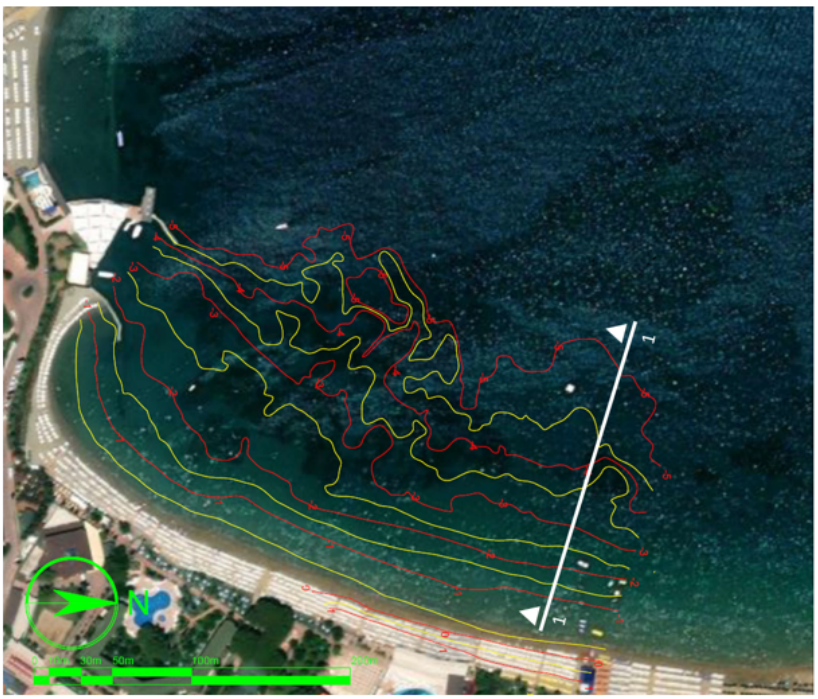

Figure 4.2. Bathymetry of the measurement site.

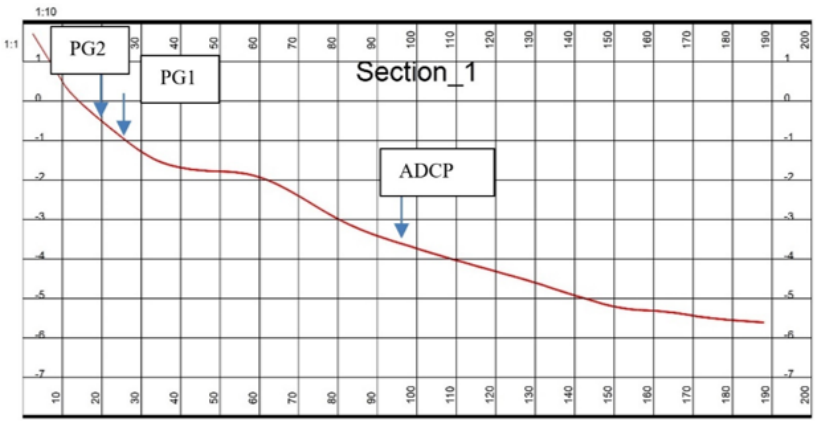

Figure 4.3. Scaled test section.

4.3. Field Measurement Method

As the PO leaves move randomly in nature, it is impossible to locate the measurement devices at the path of the PO motion before they start moving. Therefore, it was planned to perform the tests in a "semi-controlled" condition i.e., PO leaves are trapped in a zone and subjected to real sea waves and bathymetry. The steps of testing are provided below:

- Step 1: Test location is identified as a shore-normal band where the seabed has the typical slope of 1/30 and a form without any irregularity.
- Step 2: Washed ashore PO leaves along the same beach are transported to test site via land transport.
- Step 3: Measurement devices are deployed at the seabed at pre-identified locations.
- Step 4: A fishnet is installed in the cross-shore direction to keep the PO leaves within the testing area.
- Step 5: PO leaves are manually transported to the testing area in a canoe and released to the water.

Below listed equipment is used during measurements:

- Acoustic Doppler Current Profiler (ADCP) with 1MHz beam frequency
- Two Pressure Transducers
- Conductivity, Temperature, Depth measurement device (CTD)
- Survey Equipment
- Level Measurement Equipment
- Single Beam Bathymetric Echo-Sounder
- Drone
- Boat (Gezgin) with 60 HP engine.

Our aim is to measure the wave heights at three different locations in the cross-shore direction. These are: (a) deep water to measure the incident wave characteristics, (b) shallow water where the waves have not passed the PO covered area and (c) shallow water after the waves pass the PO covered area. An acoustic doppler current profiler (ADCP- 1 MHz) and two pressure gauges (PG1 and PG2) are deployed in a row in the shore-normal direction. Prior deployment of the devices, calibration done for each device in Boğaziçi University Coastal Engineering Laboratory, Istanbul, Turkey (Figure 4.4). ADCP sampling rate is set to 2 Hz for pressure measurement and 4 Hz for acoustic surface tracking (AST). ADCP operated in bursts of 17 minutes of continuous recording and 13 minutes of sleeping mode. Each data burst contains 2048 pressure data and 4096 AST data. The two custom-made pressure gauges (PG1 and PG2) recorded continuously at 4 Hz without sleeping mode with a built-in capacity of 1.2 million records (83 hours of data). Device locations are provided in Table 4.1. General site installation and ADCP position under water and can be seen in Figure 4.5 and Figure 4.6 respectively

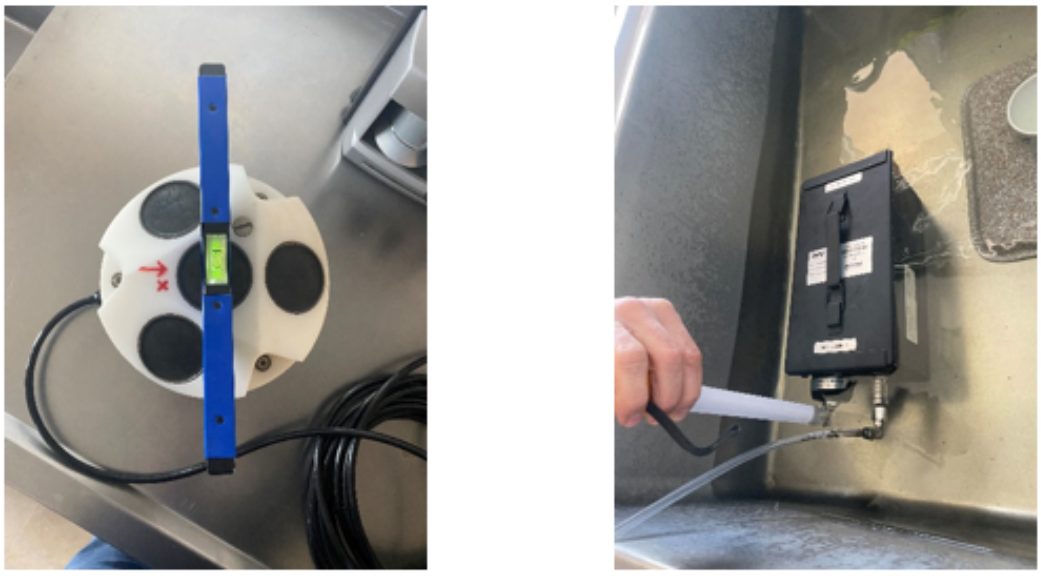

Figure 4.4. Calibration of measurement devices (a) ADCP (b) Pressure gauge.

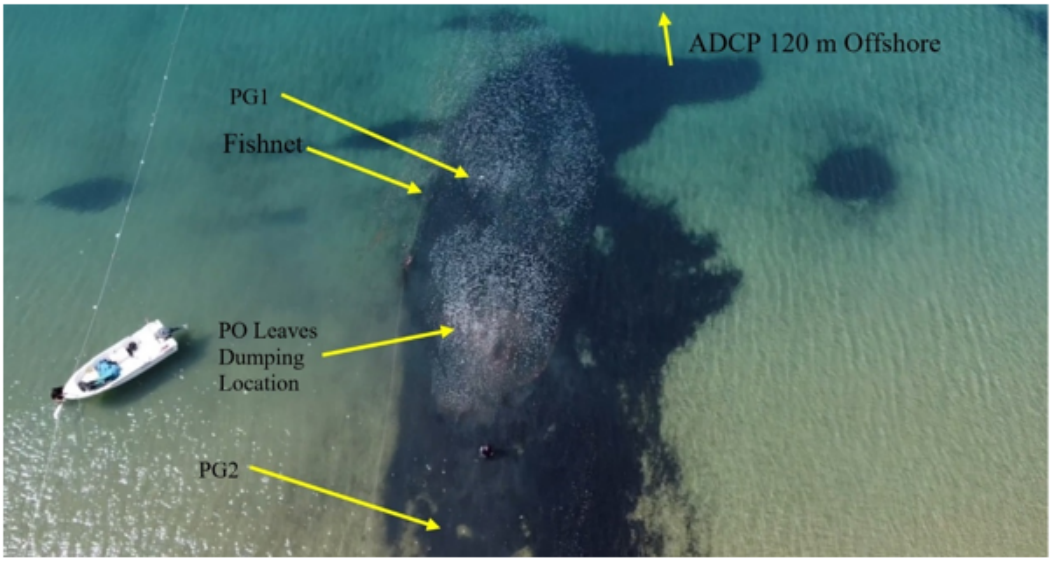

Figure 4.5. Test setup and device locations.

Figure 4.6. ADCP Device installed under water.

Table 4.1. Measurement device locations.

	Northing [m]	**Easting [m]**	**Device Installed**
St 1	390.332.749	4.053.887.423	Acoustic Doppler Current Profiler (ADCP)
St 2	390.426.312	4.053.866.927	Pressure Gauge 1 (PG1)
St 3	390.440.026	4.053.864.256	Pressure Gauge 2 (PG2)

Conductivity, salinity, and density measurement of the seawater was done with an oceanographic measurement device. Average conductivity at the time of site test were measured 50.1 mS/cm. Salinity and density is measured as 39.09 PSU and 1028.4 kg/m^3 respectively. Average measured sound velocity is 1520 m/s. Density measurements were done in laboratory to the samples collected from the site. Pycnometer results indicate 0.999 kg/m^3 density of PO leaves which is lower density than seawater. However, once they were released to the test location most of the leaves sunk to the bottom owing to adhered sand particles to the leaves which made them heavier than the seawater.

Washed ashore PO leaves are collected from the beach and brought to the measurement site by truck. The PO leaves are then loaded to a canoe, carried to the target location, and gradually released between the two pressure gauges (PG1 and PG2) continuously for four hours at a constant pace until the entire amount of 27 m^3 of PO leaves are used (Figure 4.7). Some of the PO leaves washed ashore during the testing and some of them escaped the testing zone. The PO leaves piled up between PG1 and PG2, reaching up a maximum height of 15 cm at the sea bottom. As shown in Figure 4.8, at the end of the measurement, the PO leaves are distributed both in longshore and cross shore directions. The measurements are continued until several hours after terminating the PO release, so that the remaining PO leaves between PG 1 and PG 2 are reduced to a minimum and do no effect the wave parameters any further. The findings on how the leaves interact with the incoming waves are detailed in Chapter 6.

Figure 4.7. Barrow area of PO dead leaves and testing location.

Figure 4.8. Testing location after completion of test and PO leaves left the zone.

4.4. Data Analysis

In addition to the underwater electronic wave recorders, aerial drone images are used to track the PO motion. With the help of a video editing software, the drone images are also used to measure the durations between two consecutive wave crests measured at a fixed location within the test site. These visually measured peak wave periods are used to apply bandpass filters to the spectral analysis of the wave data for narrowing the focus of the wide range of periods of waves measured with electronic devices. As it can be seen in Figure 4.9a and b, the wave period is measured as 5 s.

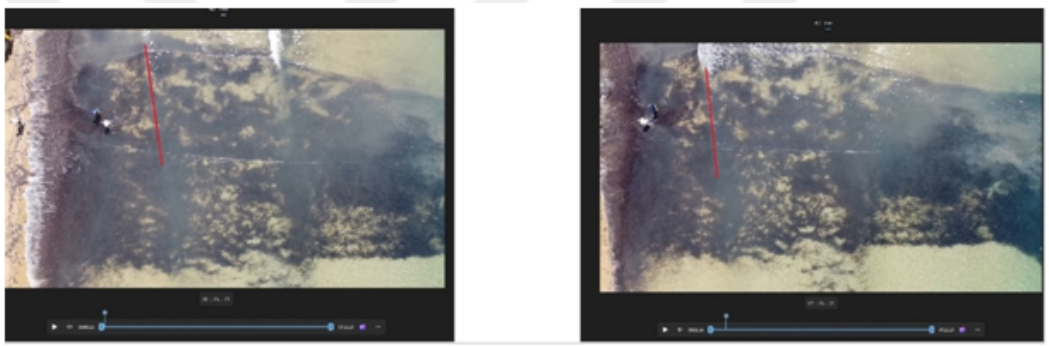

Figure 4.9. Wave crest positions at the same location (a) t=0 s. (b) t=5 s.

The video frames in Figure 4.10, shows the distortion in wave crests due to the presence of PO leaves within the testing zone in the form slowing down the wave celerity and the retardation of wave breaking inside the PO zone. This is a clear indication that PO leaves have a considerable impact on wave propagation and the transmission of wave energy flux.

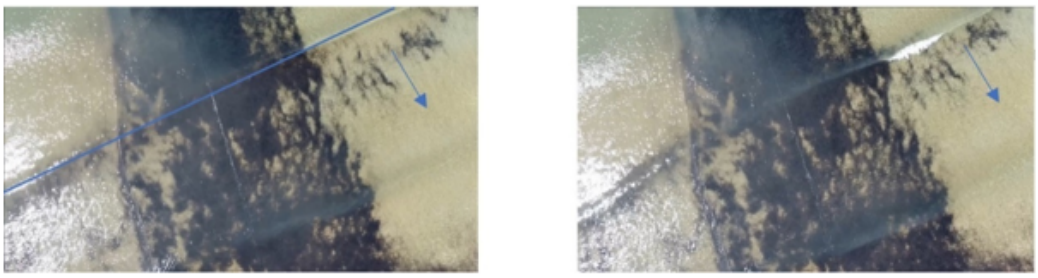

Figure 4.10. Wave crest distortion due to PO dead leaves.

Raw data collected at ADCP and pressure gauges is processed both in time and in frequency domains. Each burst of the raw data consists of 2048 records at a sampling frequency of 2 Hz. To improve the resolution, each burst is split into two in the analysis. Raw data is processed using Fourier Transform (FT) with MATLAB Software. Once the time series data is transformed into frequency domain via FT, spectral density functions are calculated using the formula below

$$X(t) = f(\eta, t), \tag{4.1}$$

$$X(f) = FX(t), \tag{4.2}$$

$$(f) = \frac{1}{T}|X(f)|^2, \tag{4.3}$$

where $X(t)$ is the time history function of the recorded sea level elevations, $X(f)$ is the water surface elevation in frequency domain and F, denotes for Fourier Transform, f is the frequency in Hz and $S(f)$ spectral density function and is the sea surface elevation. The characteristic wave parameters are obtained from the spectral density function using its zeroth and higher order moments as follows

$$m_n =_0^{S(f).f^n.df,} (4.4)$$

where, m_n is the nth order moment of the spectral density function. For $n = 0$ we get m_0 which is the zeroth moment of the spectral density function

$$m_0 =_0^{S(f).df.} (4.5)$$

Physical interpretation of m_0 is, area under the spectral density function which is also variance of spectrogram. Higgins, L (1952), approximated the significant wave height, H_{m0}, with m_0 with below formulation [34]

$$H_{m0} = 4\sqrt{m_0}. \tag{4.6}$$

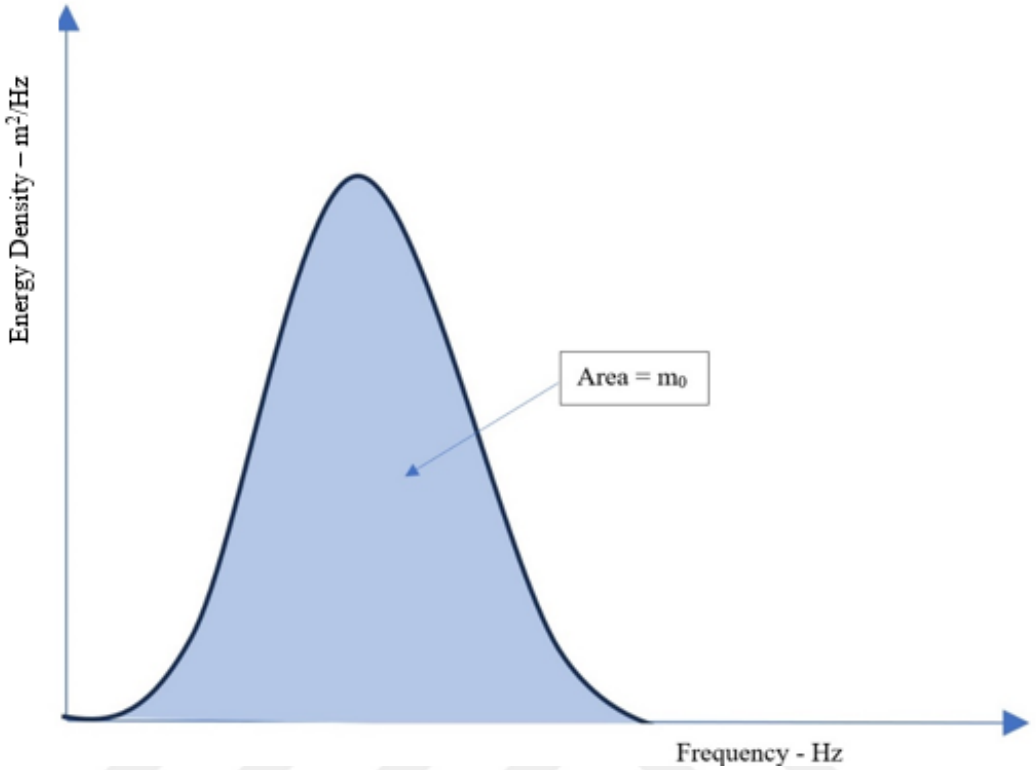

Figure 4.11. Spectral density function sketch.

Many other statistical wave parameters can be obtained from the spectral density function. The mean wave period, T_{m02}, is given with an approximation

$$T_{m02} = \sqrt{\frac{m0}{m^2}}, \tag{4.7}$$

where, m_0 is the second moment of the spectral density function.

With a sampling frequency of 2 Hz, the Nyquist frequency for Fourier Transform analysis is 1 Hz, which is half of the sampling rate. To eliminate high-frequency noise in the wave data, a band-pass filter ranging from 0.1 to 0.3 Hz (corresponding to wave periods of 3.3 to 10 seconds) is used in the spectral analysis. This range covers the periods for the most common water waves, ensuring that the analysis focuses on the relevant wave periods.

Under progressive waves, measured pressure values are the combination of static and dynamic pressures. To calculate the wave induced water level fluctuation the following formulation is used

$$p = -\rho g z + \rho g \eta K_p, \tag{4.8}$$

where, p is the measured pressure, ρ is the density of the sea water, z is the depth of the sensor from mean sea level, and K_p is the dynamic pressure compensation factor given by Dean and Dalrymple (1984) with below formula [15]

$$K_p = \frac{coshk(h+z)}{cosh(kh)}, \tag{4.9}$$

where h is the depth of the seabed from mean sea level, k is the wave number and z is the vertical coordinate of the pressure device location with origin at the mean sea level and negative downwards. The water surface fluctuation in frequency domain, $\eta(f)$, is calculated by plugging Equation (4.8) into Equation (4.9) with the following equation:

$$\eta(f) = \frac{p_D(f)}{\rho g cosh(k(f)h)}, \tag{4.10}$$

where d is the depth of device below the mean water level and $p_D(f)$ is the dynamic pressure in frequency domain which is the second term in the right side of Equation (4.8). Since, analysis is performed in frequency domain via FT, $k(f)$ is the wave number in frequency domain and $\eta(f)$ are the Fourier Amplitudes. Inverse Fourier Transform is performed to get $\eta(t)$

$$\eta(t) = F^{(-1)}\eta(f). \tag{4.11}$$

In the FT analysis, the wave dispersion relation is used for each period (or frequency) value. For the dispersion equation solver, Vatankhah and Aghashariatmadari (2013) explicit formulation is used to calculate the kh values for entire frequency band [35].

The effect of PO leaves on wave height is evaluated using the variation of H_{m0} values between the measurement devices which is quantified as the transmission coefficient (K_t) calculated for each burst as

$$K_t = \frac{H_(m0 - shallow)}{H_(m0 - deep)}, \tag{4.12}$$

where $H_{(m0-shallow)}$ and $H_{(m0-deep)}$ represents significant wave heights at shallow and deep locations, respectively, where we aim to calculate the transfer coefficient.

5. MODELLING

5.1. Background Wave Transformation Model – 1D

A custom made 1D transformation model is developed in order to simulate the test field as a background model in MATLAB software. Model is based on the conservation of energy flux to calculate the shoaling and refraction effects. As it is shown in Figure 5.1 energy flux is conserved between two points in a sloping beach ($F_0 = F_1$) which is both function of wave height and group velocity of waves.

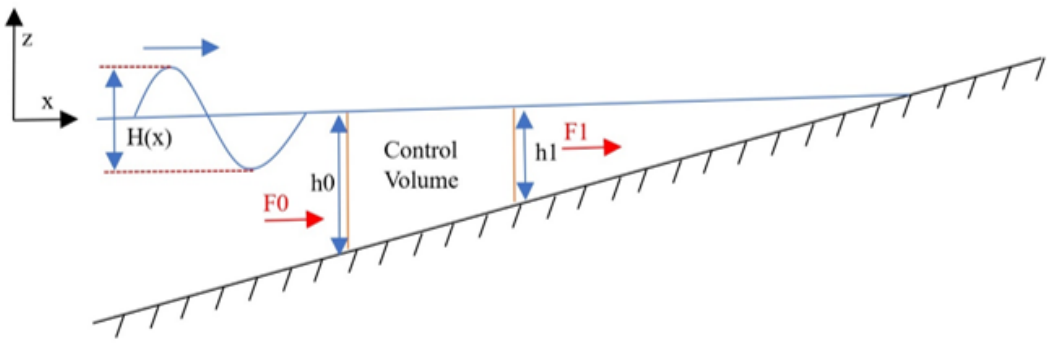

Figure 5.1. Section of beach and control volume in sloping bottom.

Below formulation is used for the shoaling and refraction coefficients

therefore
$$\frac{\partial F}{\partial x} = 0, \tag{5.1}$$

$$E_0 C_g 0 = E_1 C_g 1, \tag{5.2}$$

where E_0 and E_1 are the energy of the waves at deep and shallow locations respectively. C_{g0} denotes for the group velocity for the incident wave and C_{g1} is the same for shallow regions. since

$$E = \frac{1}{8} g \rho H(x)^2, \tag{5.3}$$

and

$$C_g = \frac{1}{2}\sqrt{\frac{g}{k}} tanh(kh) N, \tag{5.4}$$

where N is 0.5 for deep water and 1 for shallow water, and tanh(kh) is 1 for deep water, if we plug Equation (5.2) and Equation (5.3) into Equation (5.4), we get shoaling coefficient, K_s, which is

$$K_s = \frac{H}{H_0} = [\frac{2cosh^2(kh)}{2kh + sinh(2kh)}]^{(1/2)}. \tag{5.5}$$

In the same manner refraction coefficients, K_r, are calculated based on the conservation of energy with below formula

$$K_r = \frac{H}{H_0} = [\frac{1 - sin^2\alpha_0}{1 - sin^2\alpha_1}]^{(1/4)}, \tag{5.6}$$

where α_0 and α_1 are the angles between wave direction and normal to the coastline for deep and shallow water respectively. Finally wave height at any location to the onshore direction can be calculated with below formulation

$$H(x) = H_0 K_s K_r. \tag{5.7}$$

In model, above given formulation is calculated with the wave data in frequency domain and through Inverse Fourier Transform (IFT), (t) values are obtained for PG1 and PG2 stations. By working in frequency domain, transformed spectra also obtained to compare with measured data. Below formulation is applied

$$K_s(f)_i = [\frac{2cosh^2(k(f)_i h)}{2k(f)_i h + sinh(2k(f)_i h)}]^{(1/2)}, \tag{5.8}$$

$$K_r(f)_i = [\frac{1 - sin^2\alpha_0 i}{1 - sin^2\alpha_1 i}]^{(1/4)}, \tag{5.9}$$

where i denotes for each measurement data from the pressure gauge devices and, transformed sea water surface elevations are calculated with below formulation

$$\eta_i(t) = F^{-1}\eta_i(f).K_s(f)_i.K_r(f)_i. \tag{5.10}$$

5.2. Background Wave Transformation Model – 2D

Two-dimensional model was established through an open-source software. Software is used for 2D analysis of wave transformation due to shoaling, refraction, diffraction, dissipation, and wave generation by winds. Model works, with discretization of a domain into grids in two coordinates and application of finite difference method for the governing equation, which is so called “spectral wave action balance equation”. Wave action $\tilde{N}$ is defined as ratio of wave energy with respect to angular frequency and wave

action density is constant as the wave propagates in the varying sea bottom conditions. Variance in wave energy is compensated with the change in the angular frequency [36]. Spectral action balance equation given in below formulation

$$\frac{\partial \tilde{N}}{\partial t} + \frac{\partial C_g \tilde{N}}{\partial x} + \frac{\partial C_y \tilde{N}}{\partial y} + \frac{\partial C_\sigma \tilde{N}}{\partial \sigma} + \frac{\partial C_\theta \tilde{N}}{\partial \theta} = \frac{S_{tot}}{\sigma}, \tag{5.11}$$

where, the second and third term in the left side of the equation are the energy transportation in spatial directions and represents Equation (5.2) in 1D formulation. Fourth and fifth terms in the left side represent the change in the group velocity with respect to frequency and with respect to direction in spectral space. Right side of the equation is source and sink of energy which is not conserved within domain, such as wave generation by wind as source or wave dissipation by vegetation.

Based on bathymetry data measured at site, a model is established with dimension 142 m by 240 m with grid spacing of 1.5 m at each x and y coordinates. For bathymetric data in each point is generated with PDS2000 software by using the measured bathymetric data and circular interpolation was selected for calculation of the required data for model nodes. Offshore boundary location is selected as ADCP device location and data collected from the device is used as boundary values for the incident waves after processing done for spectral wave parameters. Model boundaries and grid spacings are given in Figure 5.2 and Figure 5.3 respectively.

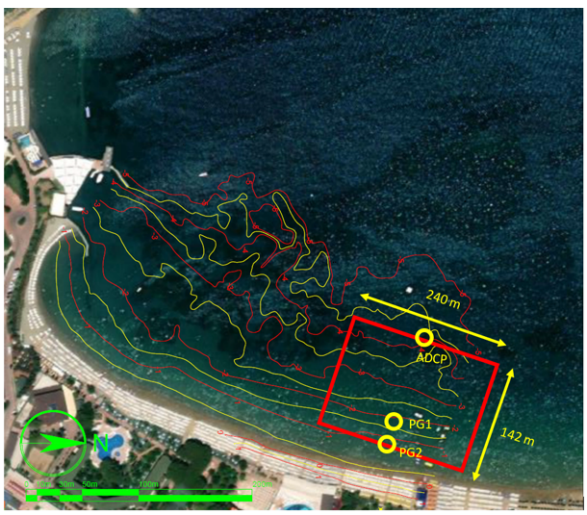

Figure 5.2. Two-dimensional model boundaries.

Model calibration was done with the data between ADCP and PG2 since the area between PG2 and ADCP was less subjected to dead PO leaves. 2D Model uses different formulations for bottom friction. We have selected Hasselman *et al.* (1973) empirical JONSWAP formulation which is given by below formulation [37]

$$S_{(ds,b)} = -C_b \frac{gk^2}{\sigma^2 cosh^2(kh)} E(\sigma,\theta), \tag{5.12}$$

where $S_{(ds,b)}$ is the energy dissipation due to bottom friction, C_b is the bottom friction coefficient, and $E(\sigma,\theta)$ is the energy which is function of and, θ. Best results are obtained with the selection of C_b= 0.04 with 3.3 % error for entire 15 measurement bursts (Figure 5.3).

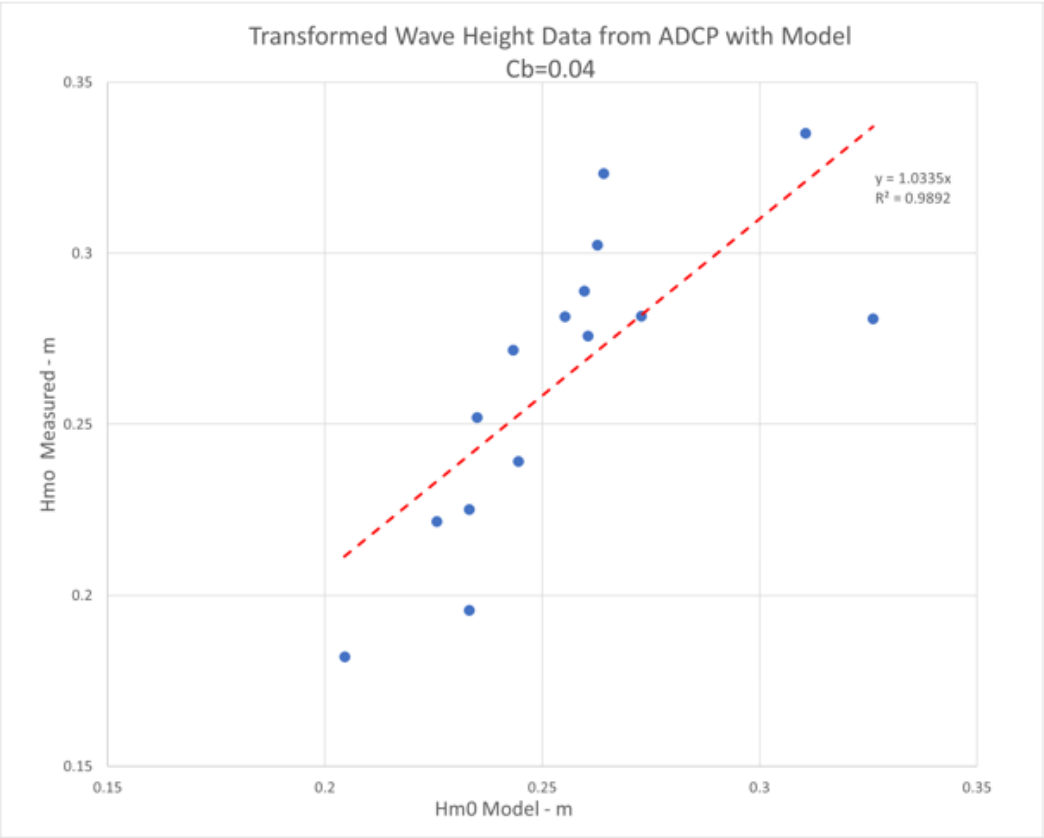

Figure 5.3. Measured wave data (PG1) vs model output with Cb=0.04.

5.3. 2D Modelling Vegetation

In the recent versions of 2D model, vegetation module is also included, and it is possible to take into account dissipation by vegetation in the model. The formulation

for vegetation is module based on the Mendez and Losada (2004) and given with below formulation which is included in the summation of the right side of the Equation (5.11) [17]

$$S_{(ds,veg)} = \frac{D_{tot}}{E_{tot}} E(\sigma, \theta), \tag{5.13}$$

where $S_{(ds,veg)}$ is the dissipation term due to vegetation and D_{tot} is unit dissipation due to vegetation and E_{tot} is the energy density. D_{tot} is given with below formulation

$$D_{tot} = \frac{1}{2g\sqrt{\pi}} \tilde{C_D} b_v N (\frac{gk}{2\sigma})^3 \frac{sinh^3(ks) + 3sinh(ks)}{3kcosh^3 kh} H_{rms}^3. \tag{5.14}$$

Equation (5.14) most of the parameters can be identified except $\tilde{C_D}$which is the bulk drag coefficient. Concept of bulk drag coefficient was explained in Chapter 2.2. This value was parameterized to calibrate the model in the presence of vegetation. It should be noted that these parameters are developed for the vegetation in the sea which are live and fixed to the bottom. In our case with the absence of mathematical model for free floating dead leaves, we tried to use the existing model and calibrate our model with bulk drag coefficient. Since our data is limited in terms of vegetation variables, we leave the derivation of mathematical model in particular for dead leaves to further studies in laboratories. In Figure 5.4, impact of $\tilde{C_D}$ on model output is presented. Although it is known that there is a linear relation between $\tilde{C_D}$ and dissipation from the formulation presented in Chapter 2, sensitivity analysis is required as $\tilde{C_D}$ is the free calibration parameter for the model. In literature, there are many correlations between dimensionless parameters and $\tilde{C_D}$, such as Re, KC and Cauchy Number. However, 2D model does not use any of those correlations and leaves the selection of parameter to the user. The reason might be all correlations provided are plant specific and wave flume specific and does not fit actual site conditions. When we have applied the relation proposed by Mendez and Losada (2004) with KC number, we obtain very less (less than $10(^{-}3)$) C_D values therefore we prefer to make the selection with trial and error [17]. Starting with 0.65 based on Figure 5.4 after many trials with the remaining burst data, C_D value of 0.55 was selected with the least error between the measured and calculated data. As the Reynold's number (Re) was calculated in the range of 4000-9000, based on literature C_D is constant for Re greater than 103 [23,26].

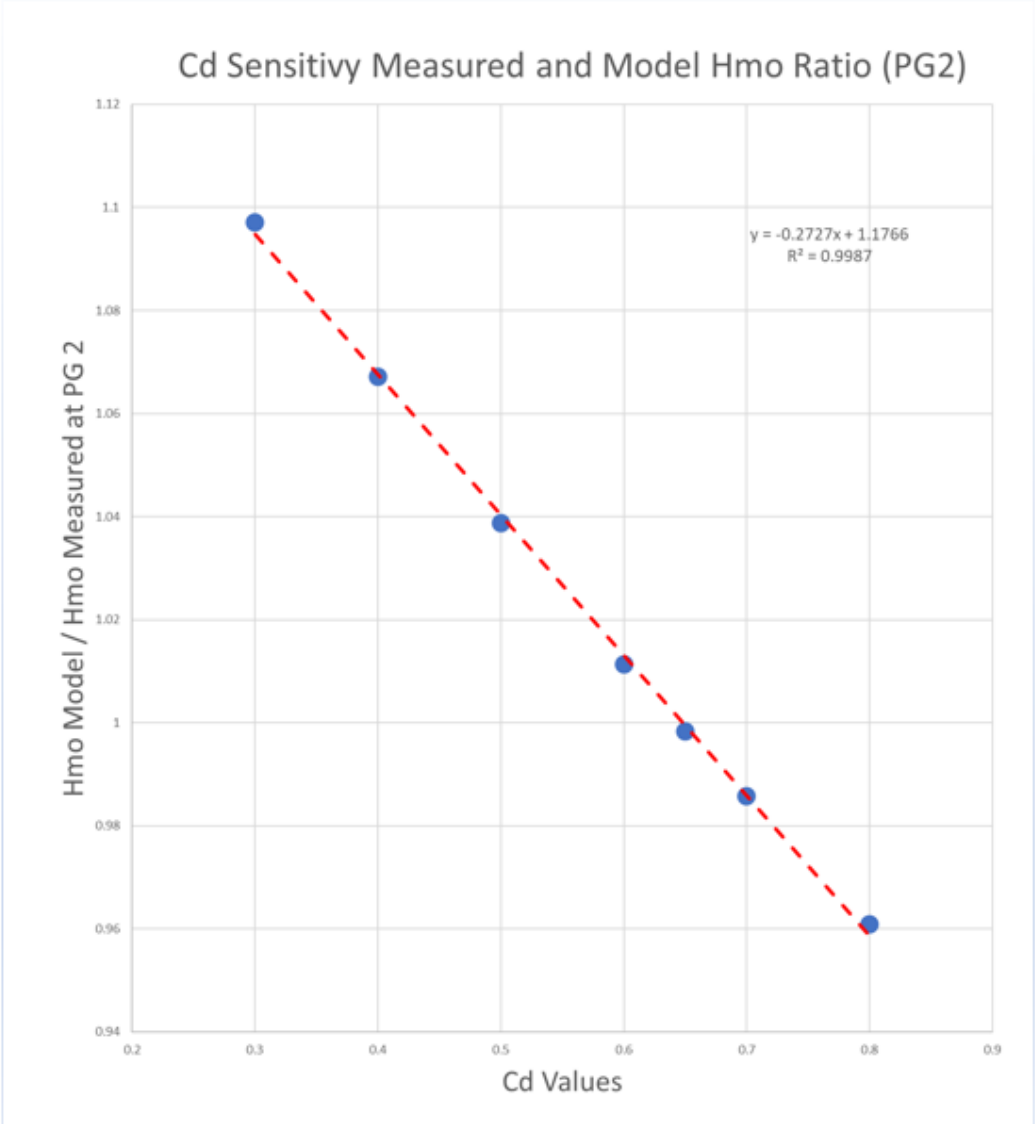

Figure 5.4. $\tilde{C_D}$ sensitivity on the measured and model result ratio for PG2.

6. RESULTS AND DISCUSSIONS

6.1. Field Test Results

Total 16 wave data bursts with each of them eight minutes of records were analysed, and the results are presented. Based on the measurement results, the dead PO leaves are found to reduce the incoming wave height by 6-27%, corresponding to a transmission coefficient of K_t= 0.94-0.73. The decay of wave energy induced by PO leaves is analysed with the energy spectra measured with ADCP, PG2 and PG1. The energy spectra of waves as the PO leaves are released into the sea are shown for Bursts 1 and 2 in Figure 6.1 and Figure 6.1b. At the initial stage of PO release, PG1 which is at the offshore side of the release point, shows a higher peak energy density compared to ADCP and PG2 due to shoaling effect. Arrows in Figure 6.1 indicate the sequence of wave transformations from offshore to onshore. In case of absence of PO leaves it is expected that the energy spectra peak values and the area under the spectra would increase as the wave approaches to the shore in shallower depth due to conservation of energy flux which is multiplication of energy with celerity. As the wave reaches to shallow water celerity reduces which is compensated increase of energy. In Figure 6.1 it is seen that the sequence of energy density is not as expected and although wave approaches to shoreline, the area and peak frequency values reduces significantly between ADCP and PG2. In Figure 6.1c and Figure 6.1d illustrate the energy spectra when the PO leaves reach the maximum concentration within the test zone where significant reduction in the energy density between incident wave (ADCP) and PG2 is observed. As the PO leaves are released between PG1 and PG2, some of the leaves are observed to disperse beyond PG1 in the offshore direction. During the later bursts as shown in Figure 6.1c and Figure 6.1d, the offshore waves become smaller (ADCP) and the shoaling between ADCP and PG1 becomes less significant. On the other hand, during these later bursts (Figure 6.1c and Figure 6.1d) since the area between PG1 and PG2 is fully covered with PO leaves, the wave energy dissipation between PG1 and PG2 is still quite significant even under such low energy conditions. It is notable here that as

the peak frequency at the initial stage of PO release was reducing while the wave is travelling from offshore to onshore direction. However, in the last burst when the PO concentration in the field is peak, ADCP and PG1 has almost same peak frequency (in other terms peak period). The shift in the peak period indicates that PO leaves dissipates some periods more than the others which will be explained in the preceding sections of this study. The energy density spectrum for the remainder of the bursts can be found in the Appendix A of this study.

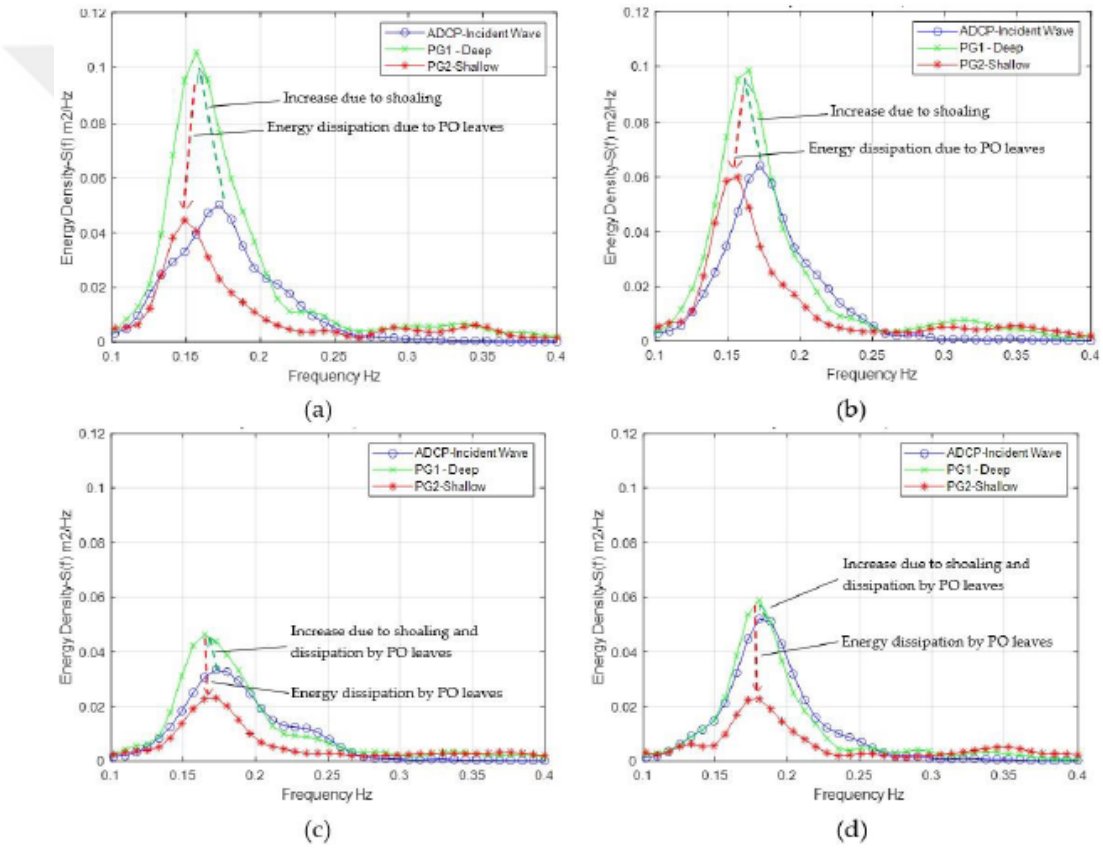

Figure 6.1. Comparison of wave spectra measured at three gauges during initial and final stages of PO release (a) 12:09 PM (b) 12:31 PM (c) 15:09 PM (d) 15:31 PM.

Figure 6.2 shows the variation of wave heights (H_{m0}) in each burst. Also detailed (H_{m0}) values for each burst and for each device is provided in Table 6.1. Regardless of temporal variations of the incident wave height, the graph shows that the gap between the offshore (ADCP) and the nearshore wave heights (PG2) first expands between 12:00 and 16:00 as the PO release continues and narrows back when the release is stopped

after 18:00. Incident wave heights vary between 0.18 to 0.26 m throughout the testing period. The peak period (T_p) of the incident waves varies between 5.1-7.3 s at both stations throughout the measurement. The mean wave period (T_{m02}) at PG2 on the other hand is approximately one second less than T_{m02} at the ADCP. This indicates that the high frequency part (short waves) in the spectrum gets filtered out as the waves pass through the PO field (Figure 6.2b). This is interpreted as the PO leaves operating like filter on the wave energy propagation, i.e., they dissipate selective dissipation on certain period or frequency waves.

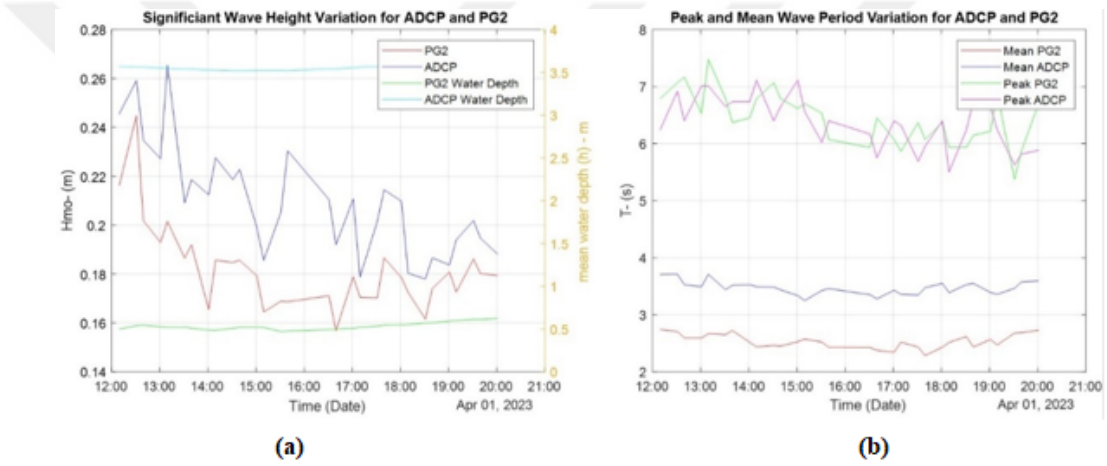

Figure 6.2. (a) Significant wave height and mean sea level variation with respect to time and stations (b) Peak and mean wave period variations.

Table 6.1. Significant wave height details for each burst.

	Start Time	**ADCP H_{mo} (m)**	**PG1 H_{mo} (m)**	**PG2 H_{mo} (m)**
Burst 1	12:09 PM	0.251	0.326	0.216
Burst 2	12:31 PM	0.266	0.311	0.245
Burst 3	12:39 PM	0.239	0.262	0.201
Burst 4	13:01 PM	0.232	0.260	0.193
Burst 5	13:09 PM	0.271	0.264	0.202

Table 6.1 Significant wave height details for each burst. (cont.)

	Start Time	**ADCP H_{mo} (m)**	**PG1 H_{mo} (m)**	**PG2 H_{mo} (m)**
Burst 6	13:31 PM	0.215	0.243	0.186
Burst 7	13:39 PM	0.220	0.272	0.192
Burst 8	14:01 PM	0.218	0.225	0.165
Burst 9	14:09 PM	0.233	0.244	0.185
Burst 10	14:31 PM	0.222	0.255	0.184
Burst 11	14:39 PM	0.227	0.259	0.185
Burst 12	15:01 PM	0.203	0.233	0.179
Burst 13	15:09 PM	0.188	0.205	0.164
Burst 14	15:31 PM	0.209	0.233	0.169
Burst 15	15:39 PM	0.237	0.234	0.169

Figure 6.3 shows the transmission coefficient, K_t, calculated as ratios of H_{m0} pairs from the three gauges (i.e., PG2/PG1, PG2/ADCP and PG1/ADCP). As expected, K_t values for ADCP/PG1 are greater than one due to shoaling as waves propagate from offshore to onshore. Part of this increase in wave height may also be due to reflection from the PO cloud onshore of PG1 as indicated by Mendez *et al.* (1998) [38]. As the waves propagate, they pass PG1 and through the PO leaves to reach PG2, the transmission coefficient drops below 1.0 to a range of 0.7-0.8 (PG2/PG1). This is a clear indication of a wave height decay due to PO leaves on the order of 20-30%. The overall wave height decay from ADCP to PG2 including the shoaling effect results with K_t between 0.94 and 0.73. The variation of transmission coefficient is mainly due to the varying PO concentration and field conditions during the testing. The net dissipation of PO leaves can be obtained by considering the wave amplification due to shoaling in the test results which obviously would result greater transmission coefficients. It should be noted here most of the literature is based on the flat bottom wave flume test which avoids shoaling impacts. In our case although the depth difference between PG1 and PG2 is only 20 cm, considering the incident wave heights ranging between 20-30 cm, shoaling of waves shall be included in the analysis for the net dissipation of the PO leaves. This subject is discussed in the preceding sections of the study.

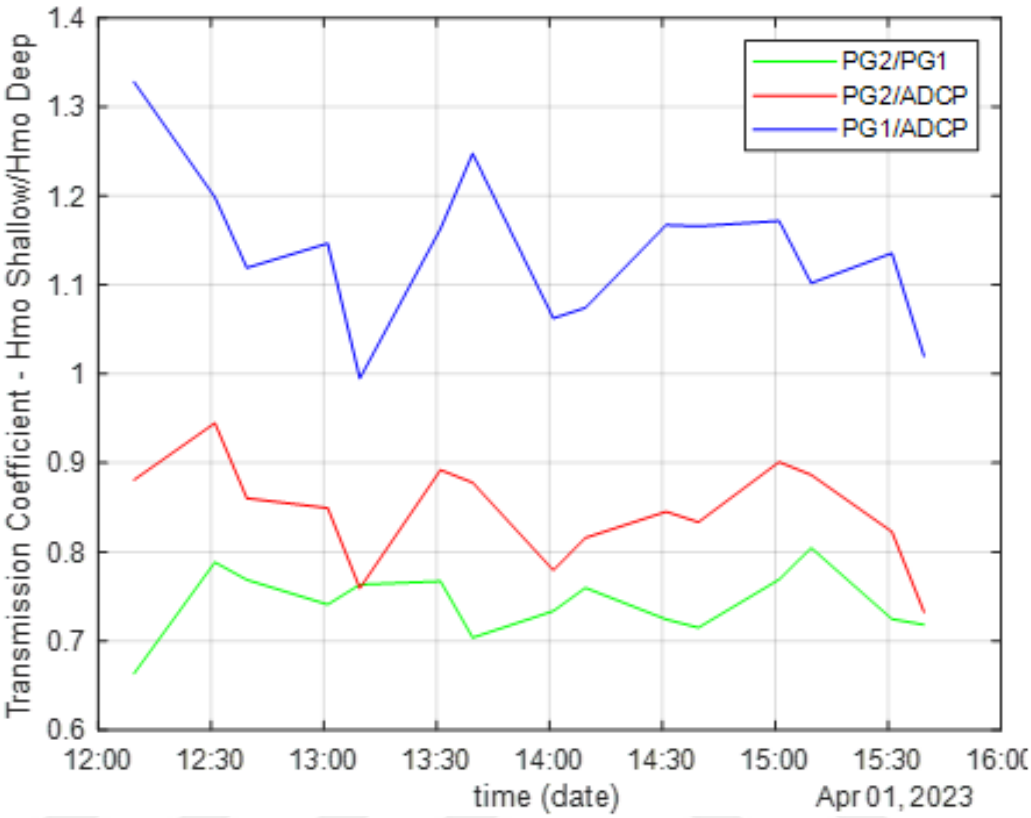

Figure 6.3. Transmission coefficient between stations.

Transmission coefficient changes as the quantity of the PO leaves within the test zone is changing (Figure 6.4). During the experiments, as the PO leaves continue to be released into the sea, the amount, and the concentration of PO leaves within the test zone increases. The graph in Figure 6.4a shows that the transmission coefficient decreases from 0.88 to 0.81 as the PO release reaches its maximum. Later, during the second half of the experiments, the PO release rate is matched and then surpassed by the rate at which PO leaves start escaping from the test area between the gauges as shown on the Figure 6.4b. Here, the transmission coefficient again increases to approximately $K_t = 0.95$ indicating a decreasing energy dissipation due to reduced PO concentration in the test area. It should be noted that the quantity of the PO leaves cannot be measured correctly within the testing zone as they are continuously transported by waves and currents. The quantities in Figure 6.4 are calculated from the volumetric estimates of the released material and uniform release rates as observed in the drone videos.

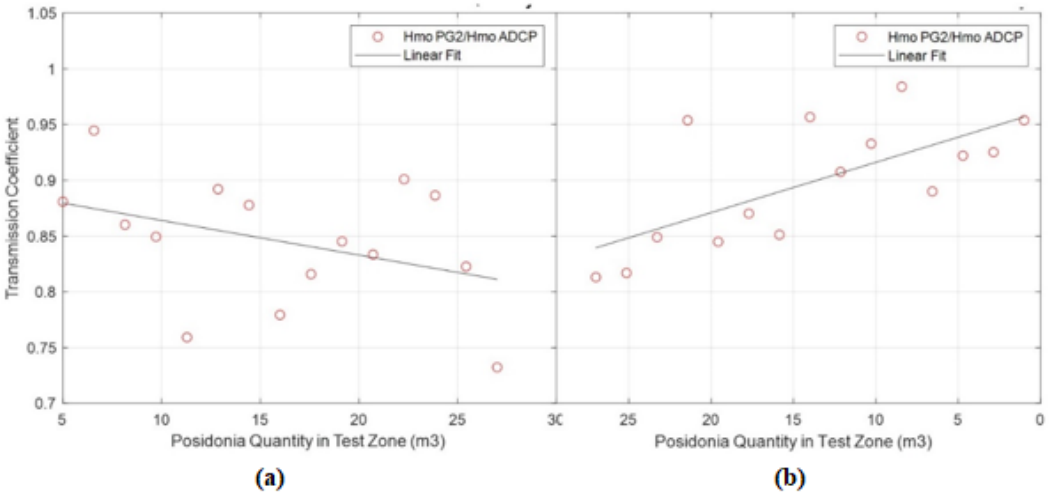

Figure 6.4. Transmission coefficient with respect to PO leave quantity within test area.

The frequency dependence of the dissipation phenomena is analysed by calculating the transmission coefficients separately for three different frequency (period) bands as shown in Figure 6.5. For each frequency band, H_m0 is calculated from the associated area of the zeroth spectral moment (m_0) within that particular frequency band and used for K_t calculation. Here, K_t values are plotted separately for long (a), mid (b) and short (c) wave periods. Each figure shows the transmission coefficients for two cases. The green line shows the wave transmission coefficient inside the PO zone (PG2/PG1) whereas the blue line shows the overall transmission including shoaling and reflection between the offshore and onshore gauges (PG2/ADCP). Long waves with periods greater than 6.2 seconds are less effected by the PO leaves (Figure 6.5a). Waves with periods between 4.6 and 6.7 seconds are strongly affected by the PO leaves with K_t values less than 0.7. In this mid frequency band, at which the peak energy is transmitted, the waves are not affected with the increased PO concentration and dissipation is observed from the early stages of the test (Figure 6.5b). Short waves with periods 3.4-4.4 seconds show the strongest dissipation by the PO field. K_t values for PG2/ADCP drop below 0.5 indicating the highest dissipation throughout the entire testing scheme. As the PO concentration is increased the leaves started to disperse offshore of the test area so that both gauges PG1 and PG2 start showing dissipation with respect to the ADCP.

Therefore, similar high K_t values are observed both in PG1/ADCP and PG2/PG1 ratios (Figure 6.5b).

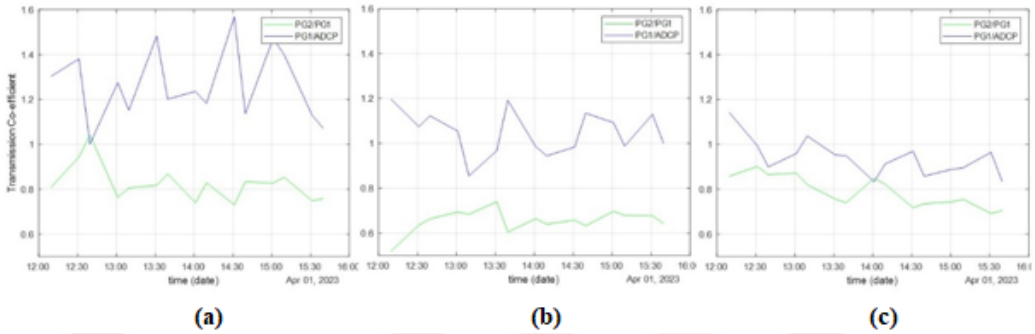

Figure 6.5. Transmission coefficients with respect to wave period (a) long periods [6.2-9.8 s] (b) mid-periods [4.6-6.2 s] (c) short periods [3.4-4.4 s].

To analyse the impact of PO leaves on various wave periods, each burst of data was segmented into one-second intervals, and H_m0 values were calculated. The analysis was performed for periods ranging from 3.4 to 9.8 seconds, corresponding to the band-pass filter applied to the wave data. Period-dependent K_t values are presented in Figure 6.6. Total 15 wave bursts were grouped into three parts based on the quantity of PO leaves present within the test field over time. Figure 6.6a illustrates the variation of K_t or the first five wave bursts with respect to wave periods. The first burst, occurring at 12:09 PM, shows a significant amount of dissipation, likely due to disturbances of the sensor at the initial stage of the PO leave release operation. However, the overall chart indicates selective dissipation by PO leaves, with very low and very high period waves remaining largely unaffected. Waves with periods between 4-8 seconds experience significant dissipation, which may be considered typical for the Mediterranean sea based on measurements available in the literature [39]. Figure 6.6b illustrates the second set of five bursts occurring between 13:31 and 14:31, during which the concentration of PO leaves within the field gradually increased. In this phase, low-period waves began to dissipate. Initially, these low-period, low-amplitude waves behaved like deep water waves (L/h $<$ 0.05, where L is the wavelength and h is the water depth), resulting in limited interaction with the deeper sections of the sea and, consequently, with the PO leaves. However, as the concentration and height of PO leaves in the water

increased, these low-period waves started to interact with the PO leaves, leading to their dissipation. Figure 6.6c presents the K_t values for the last five bursts, measured between 14:39 and 15:39. During this period, the concentration of PO leaves reached its maximum. It was observed that low-period waves also dissipated, and PO leaves acted as a low-pass filter for the wave periods. High-period waves remained almost unchanged or exhibited only minor variations between different bursts. Overall, there was a significant reduction in transmission coefficients, with an average K_t value of 0.69, indicating a 31% wave dissipation. It should be noted that the dissipation values reported here do not account for the effects of shoaling and dissipation due to bed friction.

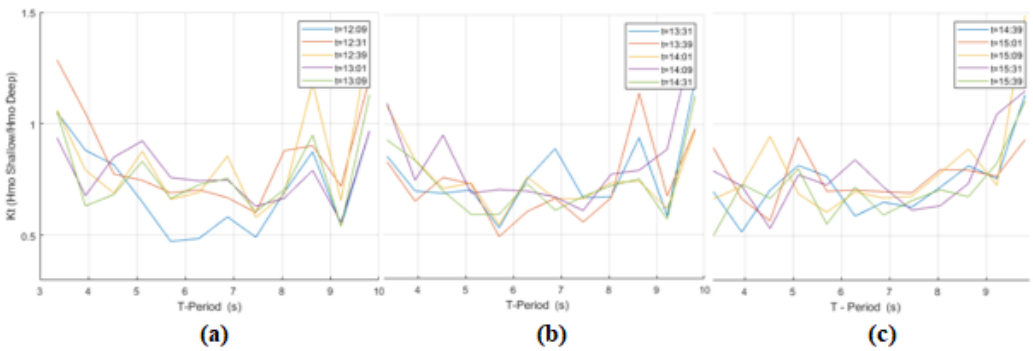

Figure 6.6. Period dependent transmission coefficients between PG1 and PG2 for wave bursts (a) 12:09-13.09 PM (b)13:31-14:31 PM (c)14:39-15:39 PM.

6.2. Model Results and Comparison with Measurements

Calibrated model is used to compare the wave transformation difference between vegetated and without vegetation cases. As mentioned in Chapter 5.2, model calibration is done between ADCP, PG 1 measurements which is practically assumed that transformation between two stations are free of PO leaves. However, during testing due to hydrodynamic effects some of the PO leaves transported beyond PG1 in the offshore side. In model calibration this impact is embedded in the bed friction co-efficient since the calibration error is minimal and can be neglected. In Table 6.2 below, model outputs based on the ADCP measurement data without vegetation is provided.

Table 6.2. Descriptives statistics of participants.

	Start Time	**ADCP**H_{mo} **(m)(measured)**	**PG1**H_{mo} **(m) (model)**	**PG2**H_{mo} **(m) (model)**
Burst 1	12:09 PM	0.251	0.281	0.275
Burst 2	12:31 PM	0.266	0.335	0.326
Burst 3	12:39 PM	0.239	0.302	0.303
Burst 4	13:01 PM	0.232	0.276	0.273
Burst 5	13:09 PM	0.271	0.323	0.312
Burst 6	13:31 PM	0.215	0.272	0.277
Burst 7	13:39 PM	0.220	0.282	0.286
Burst 8	14:01 PM	0.218	0.221	0.218
Burst 9	14:09 PM	0.233	0.239	0.234
Burst 10	14:31 PM	0.222	0.281	0.285
Burst 11	14:39 PM	0.227	0.289	0.292
Burst 12	15:01 PM	0.203	0.196	0.192
Burst 13	15:09 PM	0.188	0.182	0.179
Burst 14	15:31 PM	0.209	0.225	0.222
Burst 15	15:39 PM	0.237	0.252	0.248

As shown in Table 6.2 and Figure 6.7 the K_t values and calculated wave heights for PG1 and PG2 are too close to each other, indicating minimal variation in wave heights between stations. However, Figure 6.8, which resents the 1D model output of wave transformation, shows that the average increase in wave height due to shoaling is expected to be 7% between PG2 and PG1. When the refraction effect is included, this increase is expected to be 6.7%. This suggests that the increase in wave height due to shoaling is offset by the effects of bed friction and refraction.

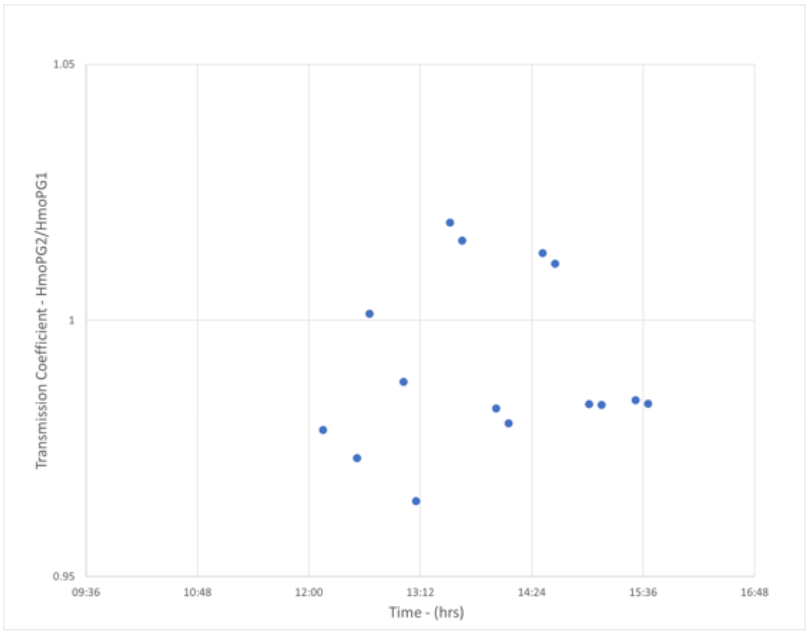

Figure 6.7. Transmission coefficient (K_t) of 2D model without PO leaves between PG1 and PG2.

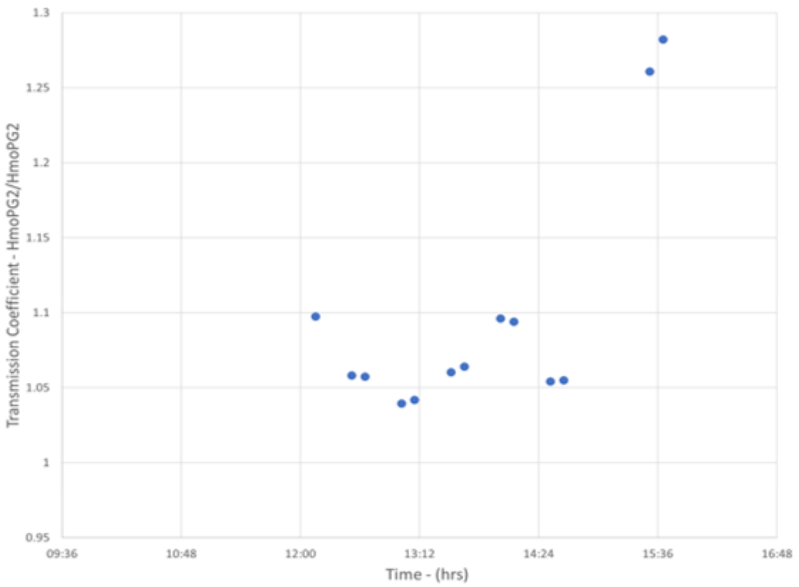

Figure 6.8. Transmission coefficient (K_t) of 1D model without PO leaves and bed friction.

1D model energy spectrum for the first burst which is at 12:09 is given in Figure 6.9 below which is a typical energy spectrum in case of non-dissipative nearshore

environment. As it can be seen, peak energy density is increasing as the wave approaches to the shore owing to the conservation of energy flux with an aligned peak frequency. The difference in dissipative environment due to PO leaves was shown in Figure 6.1 previously.

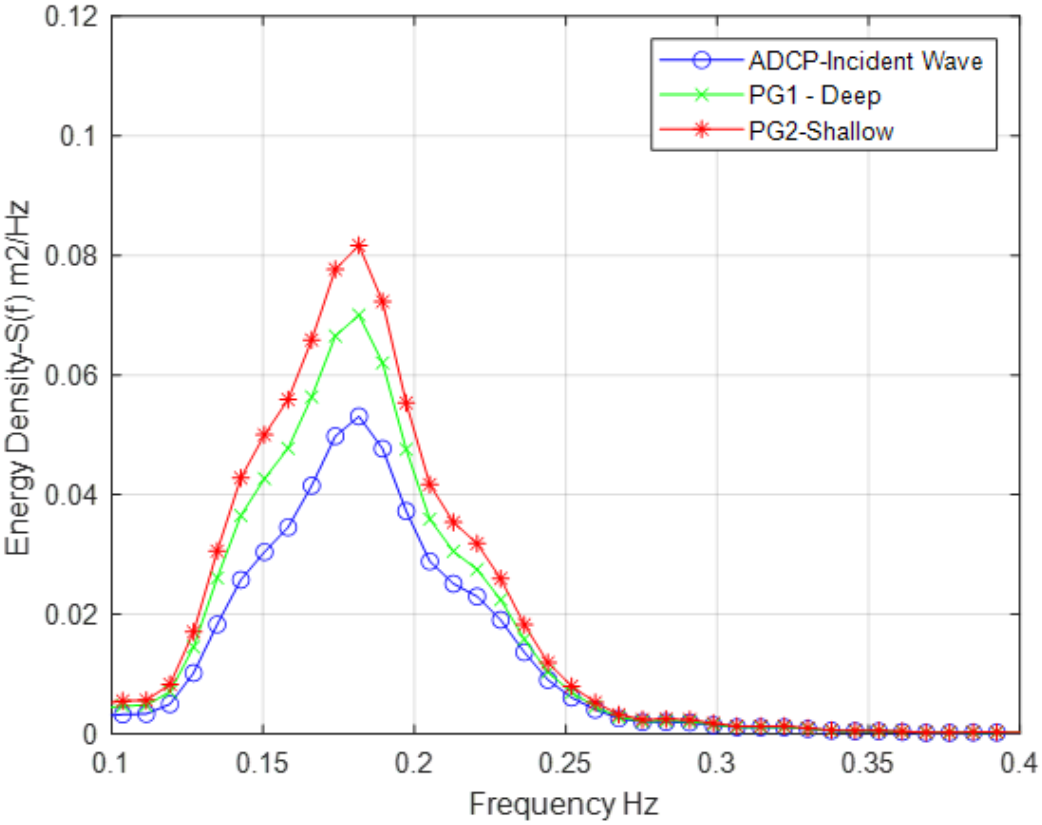

Figure 6.9. 1D model energy spectrum for the burst-1.

2D model results with vegetation and data input for the vegetation parameters are provided in Figure 6.10 and Table 6.3 and respectively. It should be noted that vegetation input parameters were selected based on Dalrymple *et al.* (1983) and Mendez and Losada (2003) which they are suitable for the live plants i.e. number of stems per unit area, plant height etc[15,17]. On the other hand, in the case of dead PO leaves the situation does not fit exactly with the literature physically as the dead PO leaves are in the state of complex cluster. Therefore, plant height considered in the input is selected as the thickness of the cluster and stem number is considered as the number of leaves per unit area. It should be note here that during field tests it is almost impossible

to measure the height and leave number precisely. Therefore, based on the random measurements within the test field and drone images and videos, approximation made on the vegetation parameters in the model and with trial-and-error method until minimum errors between measurements and model results were reached. Events noted during tests also reflected for the parameter guess. For instance, as it can be seen in Table 6.3, there is reduction in plant height and plant number between burst-10 and burst-13. During this period, PO leave release was stopped for operational reasons and such stoppage was reflected in the parameter guess as reduction of the plant number and height. Similarly, although released PO leaves increases by time, the plant height and quantity remained same as most of the time the released PO leaves are continuously transported outside test area by the hydrodynamic forces and released amount was only to keep the quantity constant in the field.

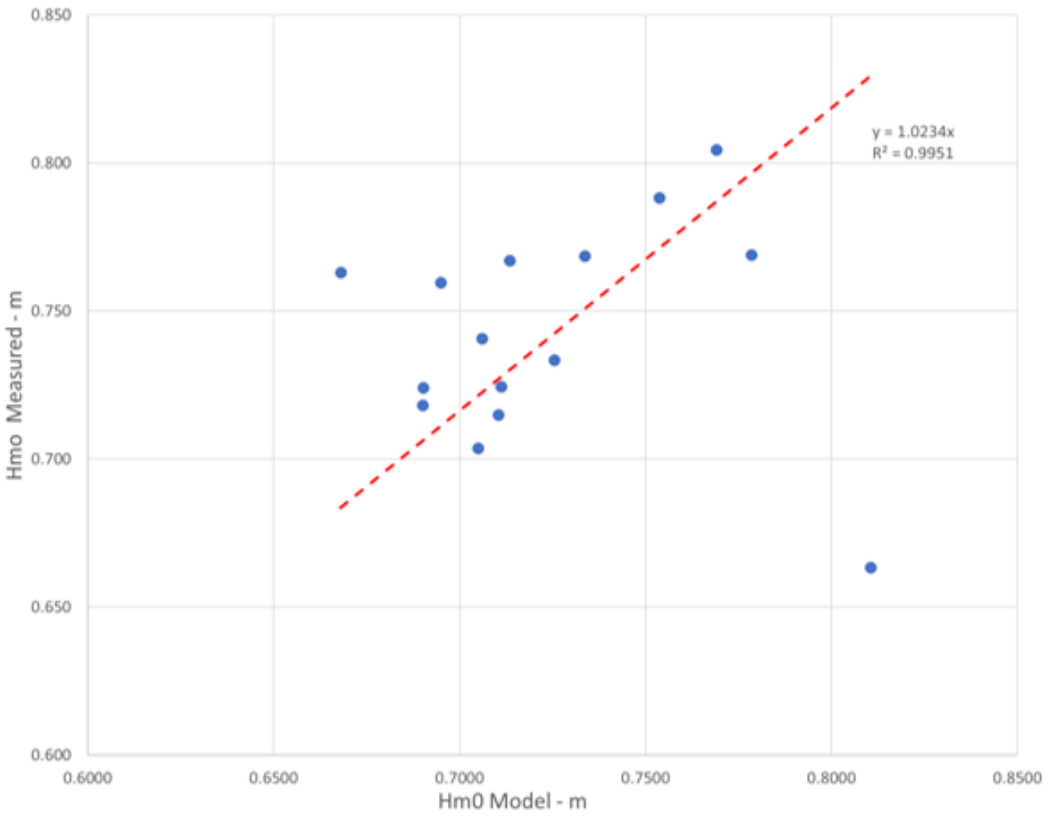

Figure 6.10. Transmission coefficient (K_t) of 2D model with PO leaves and bed friction.

Table 6.3. Model outputs for PG1 and PG2 based on the measured ADCP data without vegetation.

	N-Plant	**h-Plant (m)**	**PG1** H_{mo} **(m) (model)**	**PG2** H_{mo} **(m) (model)**
Burst 1	800	0.08	0.277	0.225
Burst 2	850	0.10	0.329	0.248
Burst 3	900	0.12	0.295	0.217
Burst 4	950	0.13	0.270	0.191
Burst 5	950	0.14	0.314	0.210
Burst 6	950	0.14	0.265	0.189
Burst 7	950	0.14	0.274	0.193
Burst 8	950	0.14	0.217	0.157
Burst 9	950	0.15	0.234	0.163
Burst 10	950	0.15	0.273	0.189
Burst 11	900	0.14	0.281	0.200
Burst 12	850	0.13	0.192	0.150
Burst 13	900	0.14	0.179	0.138
Burst 14	950	0.15	0.220	0.157
Burst 15	950	0.15	0.245	0.169

Contour views of the 2D model domain which are superposed with the satellite images for the first and last wave bursts can be found in Figure 6.11 and Figure 6.12 respectively. Red straight line in the figures indicates the path between PG1 and PG2 from offshore to onshore direction. Model successfully represent the site condition for the wave height around the testing field when compared the arial image of the field which was given in Figure 6.10. Contours around the red line in figures indicates higher wave heights whereas in Figure 6.10, waves outside PO zone (undistorted wave crest) tends to break which indicates higher wave heights as well. Rest of the contour view of other bursts can be found in the Appendix B.

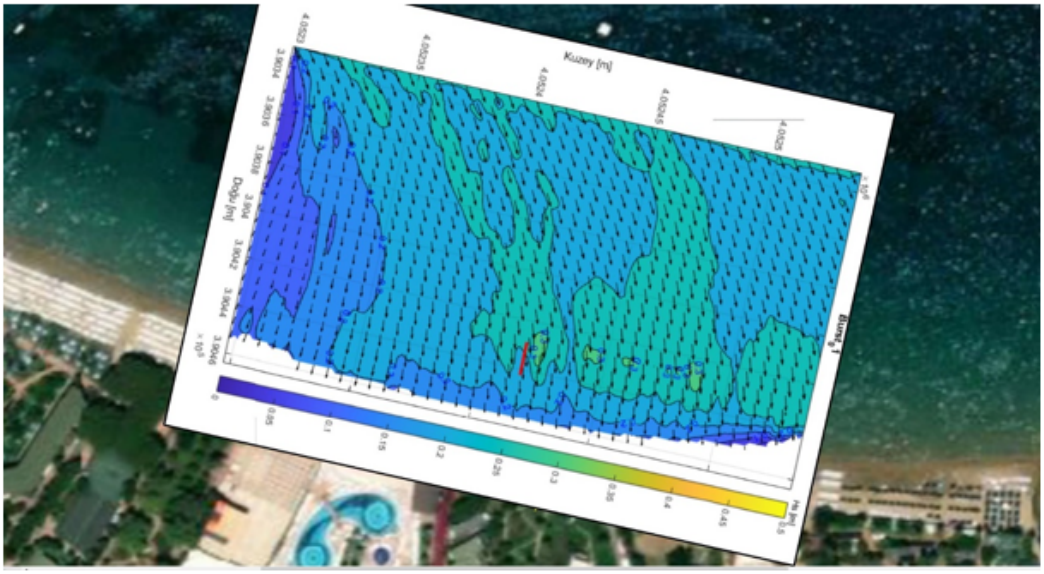

Figure 6.11. Two-dimensional model domain and contour output for wave heights for wave burst-1.

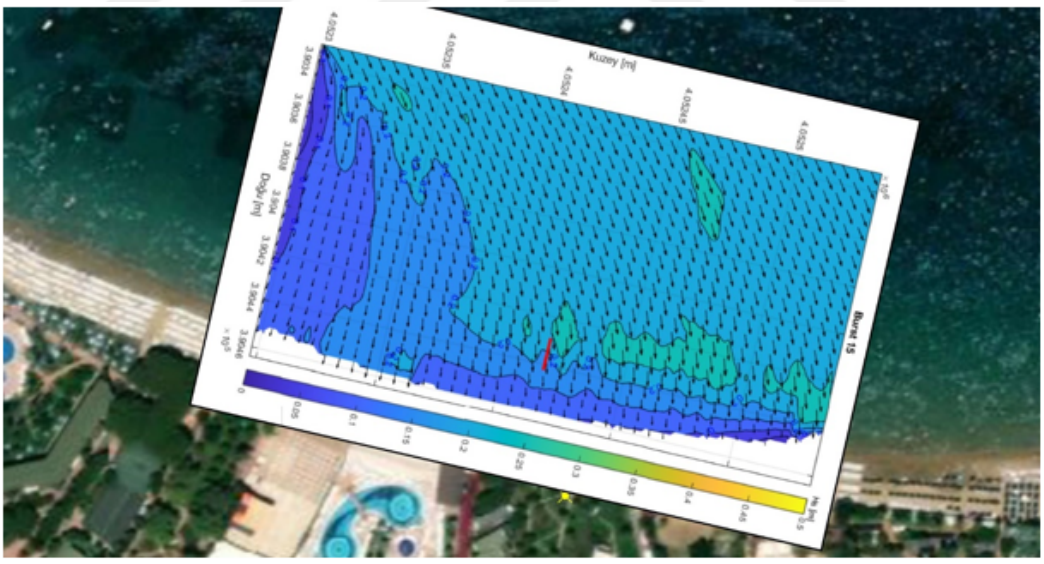

Figure 6.12. Two-dimensional model domain and contour output for wave heights for wave burst-15.

The dependence of wave attenuation on frequency or period was discussed in Chapter 6.1. This section investigates existing literature to understand the impact of wave period on the transmission coefficient. In Figure 6.13 presents the results of a 1D dissipation model based on the formulation by Dalrymple *et al.* (1983), compared

with measured data from bursts 6 to 10. Using the same parameters as the 2D model for vegetation, the Dalrymple *et al.* (1983) formula fully dissipates all the waves. To explore the period-dependent behaviour of the formulation, the plant number per unit area was reduced to identify the relationship between dissipation and wave period. A push-over analysis was conducted by increasing the plant quantity in the model. Other parameters such as C_D, vegetation height used as in the 2D model and initial wave heights are used from the measured data. Plant numbers (N) were set to 10 (Figure 6.13a), 75 (Figure 6.13b), and, 200 (Figure 6.13c). Figure 6.13a with the lowest N, the first decay observed at the period 4.7s and at periods greater than 9 s. As the N increase, decay is notable on both side of 4.7s and for periods greater than 7 s which are fully dissipated. The 4.7s is the period corresponds peak amplitude in the measurement data. We can shortly say that vegetation first dissipates peak period and large periods. This is due to derivation of Dalrymple *et al.* (1983) formula which was discussed in Chapter 2.2. Dissipation formulation is derived from Morrison type equation and dissipation is correlated with particle horizontal orbital velocity in cubic. Since orbital velocity is function of wave period and wave amplitude, in 1D model dissipation starts in large period waves and at the period where the amplitude is highest [15]. Measurement data also confirms that maximum wave attenuation realized at the peak period but when large period waves are in interest measurement and model results disagree. This can be explained as in nature PO leaves are non-resistive against large velocities and may not fully dissipate the full energy of the wave. For further investigation, Figure 6.14 shows the velocity profile of the same bursts with different periods, ranging from 3.3 to 9 seconds. As seen at the level of PO leaves, 15 cm from the sea bottom, orbital velocities increase with the period. Comparing the velocity profiles, such as the first line at 3.8 seconds and the last line at 9 seconds, reveals that while the period increases 2.3 times, dissipation increases 11.3 times due to the cubic relationship between velocity and dissipation, causing velocity to reach peak values.

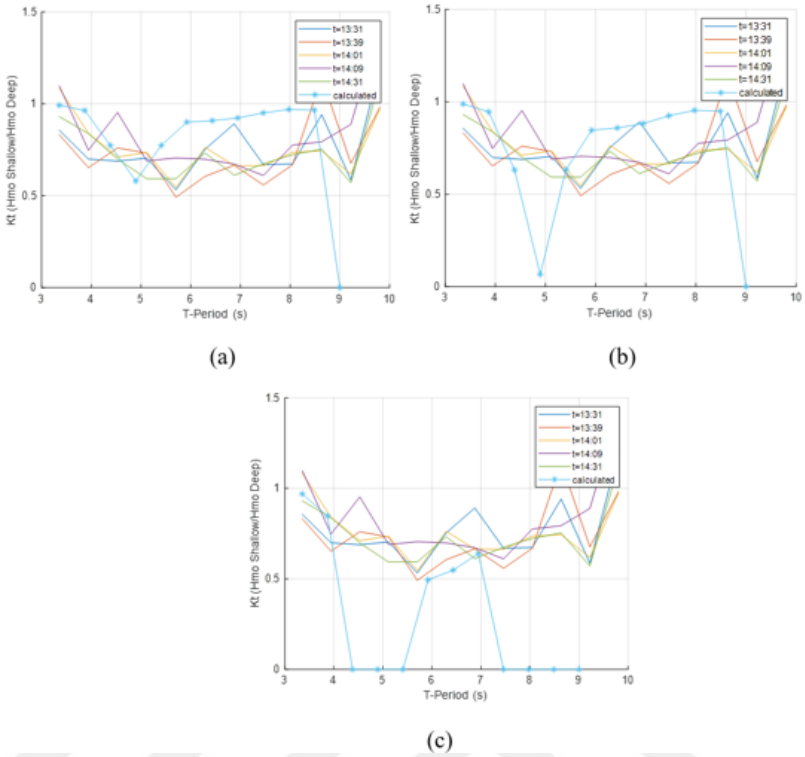

Figure 6.13. Transmission coefficient comparison between measurement and Dalrymple *et al.* (1983) 1D model for bursts 6-10 (a) N =10 (b) N =75 (c) N =200.

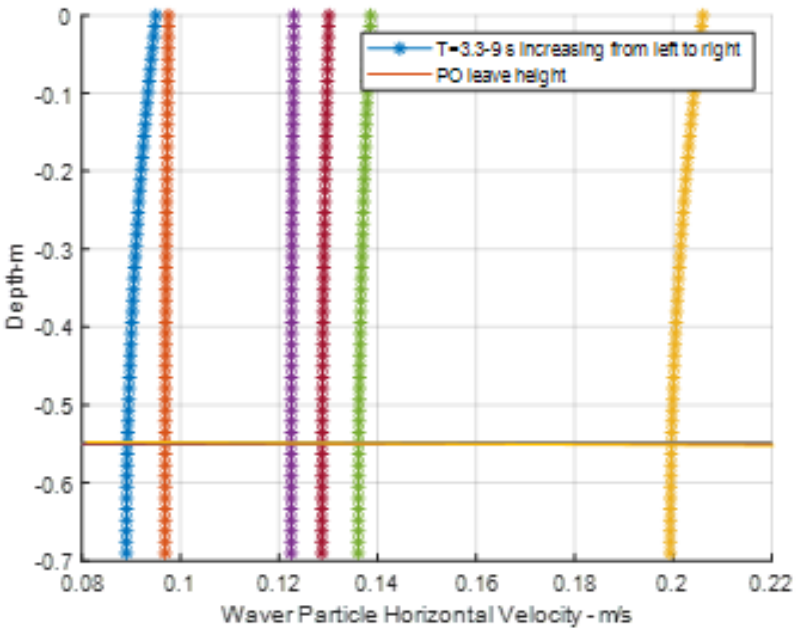

Figure 6.14. Wave horizontal orbital velocity profile for bursts 6-10.

In our case, unlike the other cases in literature which vegetation is fixed to sea bottom, the dissipation observed is much more than expected and in a broader band of period they successfully dissipate the waves. This can be explained by the complex cluster structure of PO leaves, which individual leaves have agglomerated each other and increase the relative velocity between leave and water particles. However, this structure has its limits both in the lower period and greater period side. There might be two scenarios why PO leaves fail to dissipate large period waves. First one is, due to high horizontal orbital velocity, thin blades rotate and might be aligned to flow direction which would minimize the drag forces encountered on the blades. The second scenario might be that in large period waves, the oscillatory motions are prolonged, affecting a larger path of the PO leaves within one wavelength. This could result in the cluster moving in phase with the wave, potentially reducing or eliminating the relative velocity between the water particles and the PO leaves, thereby preventing dissipation. Bradley and Houser (2009) during field test measuring the plant oscillatory motion observed similar findings that large period wave induced orbital motion are in phase with plant and showed very limited dissipation [20]. On the other hand, Nowacki *et al.* (2017) in a large-scale field measurement in a shallow estuarine, observed that high period waves dissipated more than low period waves [40]. On the low period side, we would expect quick dissipation due to frequent oscillatory motion back and forth. The reason might be the low horizontal orbital velocity allows water particle to pass through the pores without encountering PO leave blades. On the other hand, with the increase of the PO leaves, low period waves would also dissipate. As seen in Figure 6.15, which presents the last five burst during tests, low period side of the waves dissipated with the increased PO quantity while the high period side remains same. Although these results may be proof the hypothesis presented in this section further study with more dense PO leaves in more controlled environment required for final confirmation.

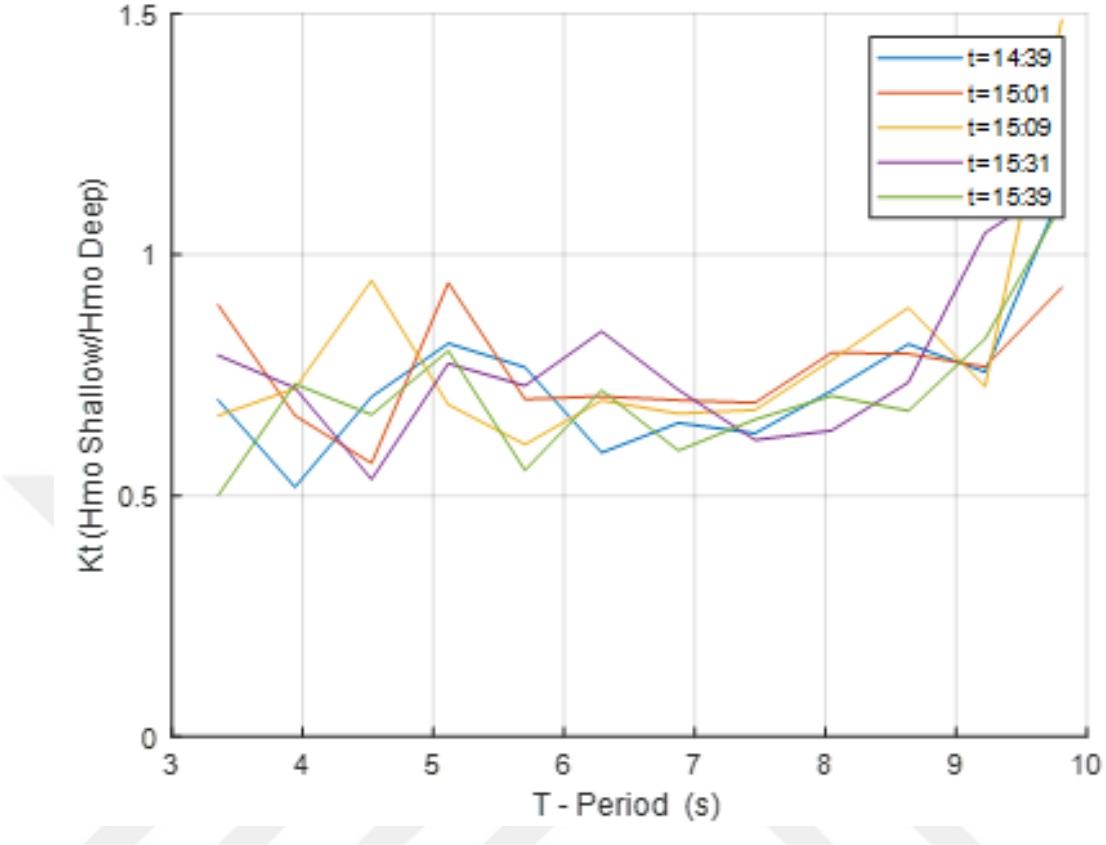

Figure 6.15. Transmission coefficient and period relation for the bursts 11-15.

6.3. Dimensionless Analysis

Analysis done with dimensionless parameters to understand the main factors driving the wave dissipation by PO leaves. As mentioned previously, Re numbers are greater than 103 therefore it is not possible to vary the drag coefficient in our analysis. Therefore, two main dimensionless parameters are selected to investigate. First dimensionless parameter is normalized wave period, T', and given with below formula

$$T' = \frac{T}{T_p}, \tag{6.1}$$

where, T, is the wave period and T_p is the peak period of the given burst. Figure 6.16 for all bursts the normalized wave period is presented with respect to transfer coefficients. Quadratic regression line was fitted to the bursts 2, 6, 8 and 15 in the order of increasing PO leaves within the test field. As seen from the figure, transfer coefficients are highly

correlated with T' suggesting maximum dissipation at the range of 0.9-1.1 regardless of the PO leave quantity in the system. As T' goes to bounds in both direction, transfer coefficient becomes more dependent to T', but more dependent in the lower bound. Because of one side dependence, regression coefficient (R^2) reduces from 0.78 to 0.5 from burst 2 to 15 which is within the acceptable range. The analysis suggests that waves with period at the range of the peak period dissipates more than others. This is in line with Dalrymple *et al.* (1983) model as the horizontal orbital velocity is a function of wave period and maximum velocity is observed at peak period which dissipates more than other period bands [15].

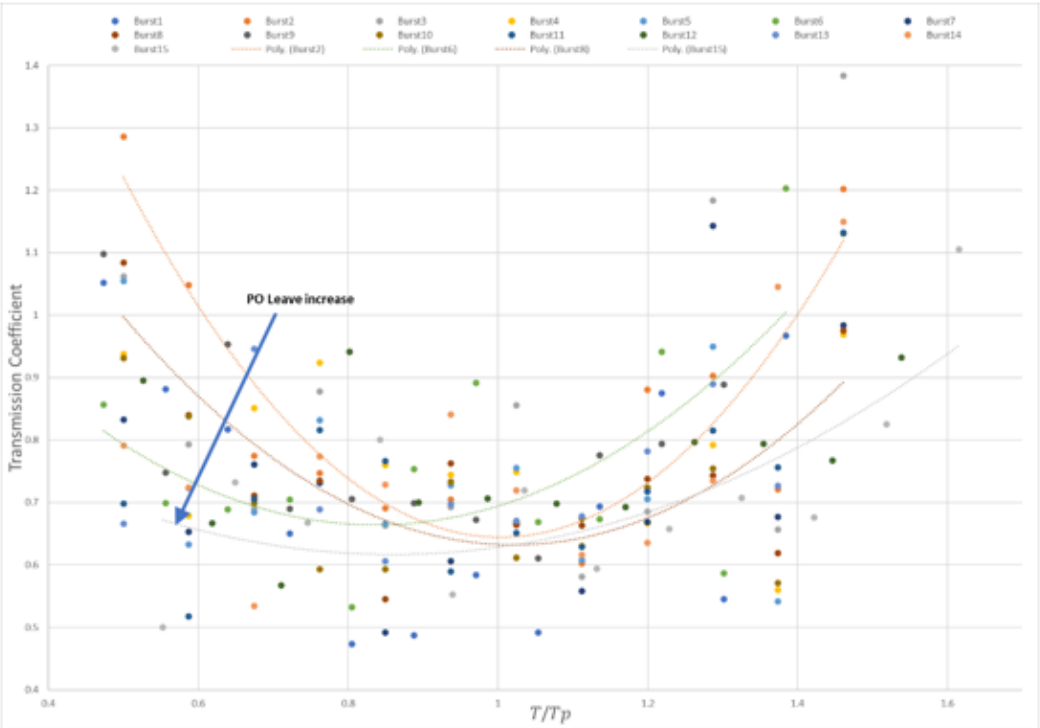

Figure 6.16. Normalized wave period for all wave bursts.

Second dimensionless analysis is the relative field length which is, length of PO leave zone in the direction of wave with respect to wave length given with the below formula

$$X' = \frac{X}{L}, \tag{6.2}$$

where, X' is the relative field length, X length of the PO zone in cross-shore direction and L is the wave length corresponding to each period band. In Figure 6.17 relative field length with respect to transmission coefficients for each burst provided. Quadratic regression lines were fit for the bursts 2,6,8, and 15. As seen in Figure 6.17 maximum dissipation observed at X'=1.17 where all of the waves dissipated more than 30 %. At X'= 1.31 is the second maximum dissipation observed with all of the bursts dissipate more than 20%. X'= 1.06 no dissipation realized which indicates that in case the wave length is more than the length of the vegetation length dissipation will not be considerable. X' values between 1.08 to 1.31 all the waves dissipated between 10 to 50% which the variation of PO quantity has minimal impact.

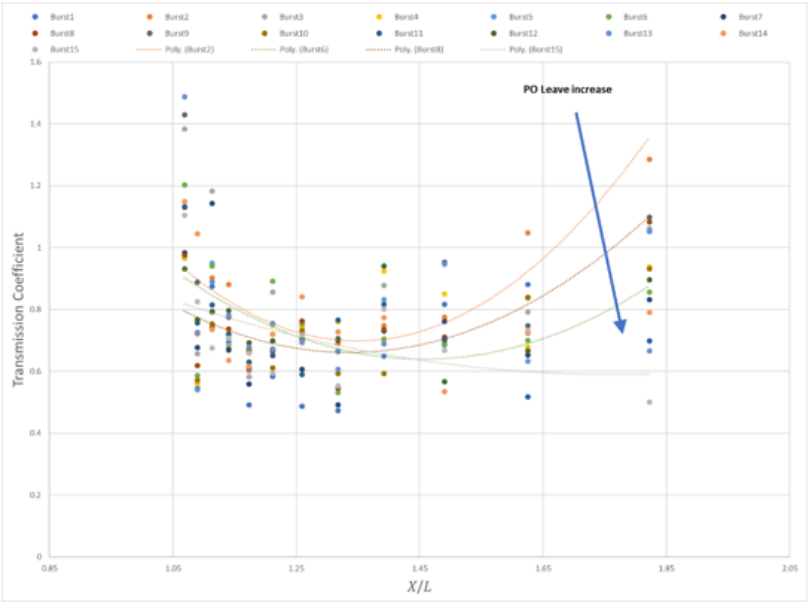

Figure 6.17. Relative PO field length with respect to transmission coefficients.

In literature, most of the studies are using relative distance of wave crest from the edge of the vegetation zone by using the same abbreviation [14,22,30,41]. Correlation with wave length versus vegetation zone usually not studied. Therefore, relative field length (X') presented here should not be mixed with the common terminology used in the literature. This finding might be important for many applications and development in engineering field, in particular in wave energy harvesting applications. Any

system should account that the system length shall be at least 20% longer than wave length of interest. It should be noted here that wave length used in the analysis is the nearshore wave lengths calculated with dispersion equation of small amplitude wave theory. Therefore, the range of the wave length is between 7.3 and 12.45 m whereas the PO leave zone within the test field or the distance between PG1 and PG2 is 13.5 m. Therefore, PO zone length in the present measurement is greater than maximum wave length. However, transformation of the waves with wave lengths greater than the vegetation zone is not known. To verify the previous statement, additional tests shall be performed. As previously discussed, this subject could be phase related between wave and PO leave motion. In case of X' greater 1.65 dissipation becomes more dependent on the leave quantity within the system. Transmission coefficients goes down to 0.5 depending on the PO leave quantity which is the maximum at burst 15. In burst 15, the variation of the transmission coefficients is not quadratic. As shown in Figure 6.18 the relation between X' and K_T can be modelled as a rational function with singularity around X'= 1.05.

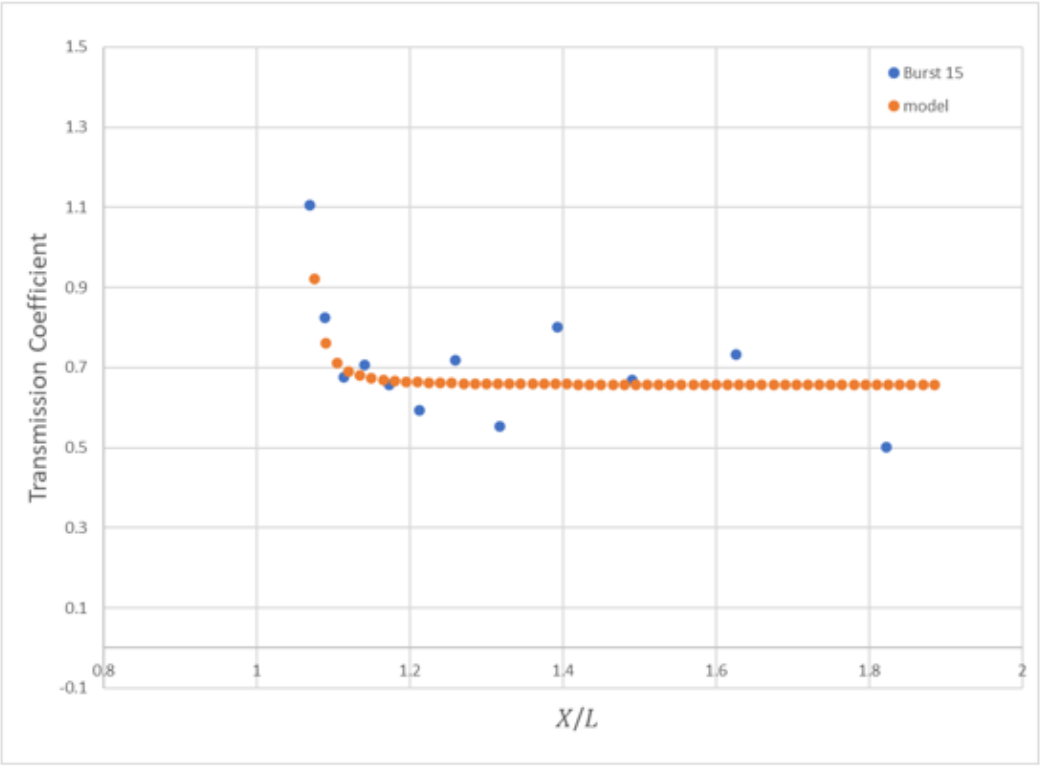

Figure 6.18. Transmission coefficient and X/L measurement and model plot.

The model given in Figure 6.18 is given with below formulation

$$K_t = \delta + (\frac{\beta}{1.05 - X'})^2, \tag{6.3}$$

where, δ and β constants depending on the PO leave concentration parameter, α, which is given with below formulation

$$\alpha = Ns, \tag{6.4}$$

where, N is the number of PO leave per unit area and s is the height of the cluster. A and B constants are determined by numerical iteration by using the measured K_T and X' values for each burst. In Table 6.4 below, δ and β values with regression value of the R^2 can be found. R^2 values are calculated by the ratio of regression sum of squares and total sum of squares. Correlation with the model increases as the PO concentration increase. For instance, in burst 13 the correlation is 82% which is quite satisfactory.

Table 6.4. δ and β constants, α and R^2 values for each burst.

	δ	β	α	R^2
Burst 1	0.677	0.010	0.064	0.12
Burst 2	0.811	0.011	0.085	0.21
Burst 3	0.776	0.014	0.108	0.44
Burst 4	0.739	0.010	0.124	0.05
Burst 5	0.733	0.011	0.133	0.29
Burst 6	0.713	0.013	0.133	0.50
Burst 7	0.696	0.010	0.133	0.22
Burst 8	0.724	0.010	0.133	0.13
Burst 9	0.761	0.015	0.133	0.66
Burst 10	0.691	0.012	0.143	0.47
Burst 11	0.679	0.013	0.126	0.71
Burst 12	0.730	0.010	0.111	0.18
Burst 13	0.707	0.016	0.126	0.82
Burst 14	0.718	0.013	0.143	0.60
Burst 15	0.657	0.013	0.143	0.72

Dependency between δ, β constants and α with respect to with α is plotted in Figure 6.19 and Figure 6.20 respectively.

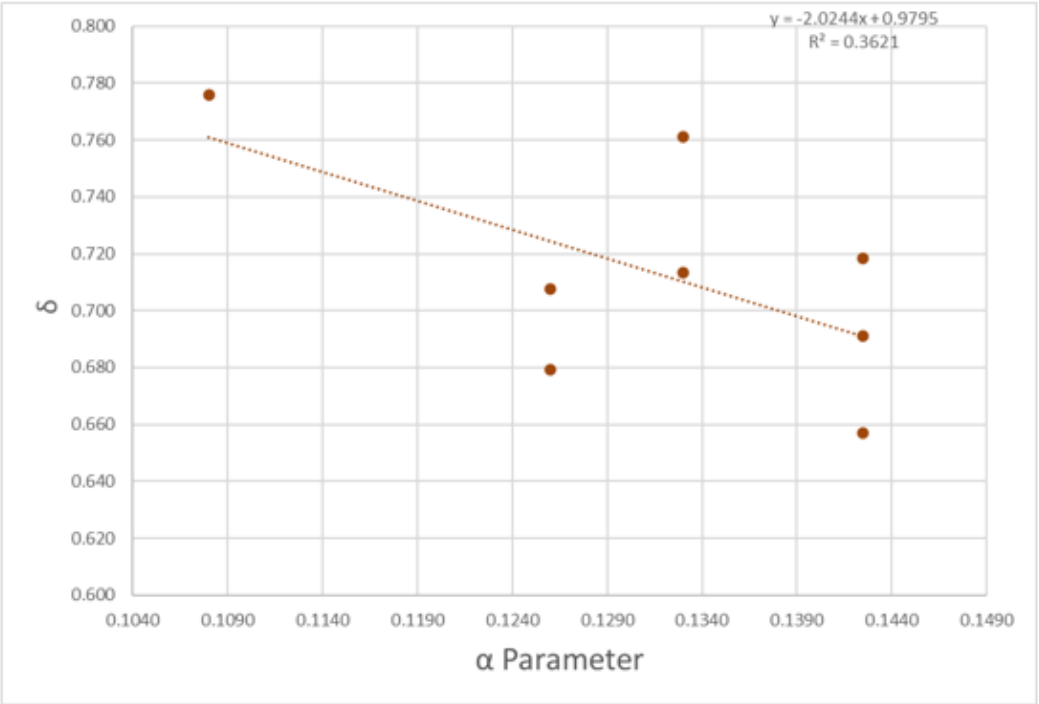

Figure 6.19. δ constant with respect to α.

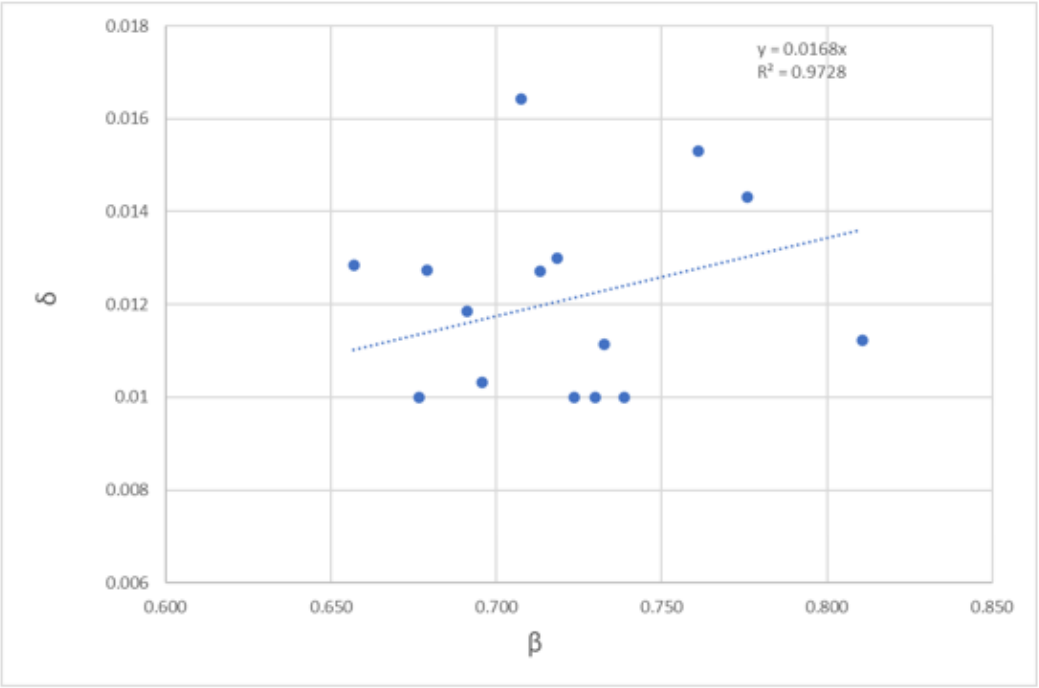

Figure 6.20. δ and β relation.

Based on Figure 6.20 below δ can be calculated by using the linear fit formulation

$$\delta = -2.02\alpha + 0.98, \tag{6.5}$$

$$\beta = 0.017\delta. \tag{6.6}$$

By using Equation (6.3), Equation (6.5) and Equation (6.6) we can calculate the wave transmission coefficient and therefore wave dissipation of PO leaves in shallow waters. It should be noted here that while preparing Figure 6.19 wave bursts which has R^2 greater than 0.4 were accounted which are eight bursts out of 15. The reason of weak correlation in other burst is due to semi controlled setup of the test field as we were not able to measure the exact quantity within the test field. Also due to operational reasons, PO concentration was limited therefore in a narrow band of values used in the correlation which is one of the main drawbacks of the formulation. In addition, the length of the test zone was limited to 13.4 m which is almost one wave length of the largest period in nearshore. Equation (**??**) can be extended with tests with longer test zone and more concentrated PO quantity which left for future studies. Verification also can be done in wave basins with real PO leaves within more controlled environment.

7. CONCLUSION AND FUTURE STUDY

7.1. Summary and Conclusion

Wave energy is the main factor for sediment transport in both cross-shore and longshore direction and therefore beach erosion as well. NBS solutions are area of interest for many researchers owing to its cost and environmental benefits. It is hypothesised in this study that dead free floating PO leaves dissipates the wave energy and contribute for beach development by reducing the eroding forces. This is based on Author's observations in the fields. To prove the hypothesis a test performed in real sea conditions with dead PO leaves in the Eastern Mediterranean South of Turkey, Alanya. Testing was done in semi-controlled manner by artificially release of PO leaves in a pre-determined zone where the measurement devices were located, and waves are measured while they are passing through the PO leave cluster. Two pressure gauges in nearshore within testing zone and one ADCP in the offshore were used to investigate the wave transformation from offshore to onshore in the presence of PO leaves in the nearshore. In testing, PO leaves were subjected to sea waves during 15 bursts of approximately eight minutes of measurement at each burst. Pressure gauges and ADCP had sampling frequency of 2 Hz and total 1024 data samples for each burst were recorded. PO concentration at the field was approximated by random checks during tests and further analysis from arial images.

A transmission coefficient, K_t, is defined as the ratio of transmitted wave height divided by the incident wave height. Spectral wave parameters are obtained through Fourier Analysis of the time records including the significant wave height (H_{m0}), and the mean wave period (T_{m02}).

Transmission coefficient (K_t) was found to vary between 0.73-0.94 which is equivalent to a wave height decay of 6-27%. The results show that the free-floating dead PO leaves in their natural environment dissipate incoming wave energy and have a capac-

ity to protect the beach against erosion. Further analysis in separate frequency bands show that short waves (with periods less than 4.4 s) are more sensitive to PO leaves in terms of energy dissipation. Whereas long waves (with periods more than 6.7 s) are not sensitive. The transmission coefficient for short waves as calculated using the high frequency part of the wave spectrum, delivered a maximum transmission coefficient of 0.5 corresponding to 50% wave height decay due to PO leaves. It is concluded that the PO leaves operate like a low pass filter on incoming waves and dissipate incident short waves more efficiently. Therefore, in closed seas with shorter fetch and wave periods, the PO leaves may work as efficient as a floating breakwater which have similar transmission coefficients. The maximum transmission coefficient of 0.5 as it was found in the study corresponds to wave energy dissipation of 75 % as the wave energy is proportional to the square of the wave height. Similarly, the wave induced beach erosion may drop by 82 % because of the higher exponent in the breaker height to sediment transport relation. In addition to indirect protection of beaches, accumulated PO leaves at shore protects the beach face directly by the means of sediment trapping.

In order to decompose the other factors transforming the waves, such as bed friction, shoaling and refraction 1D and 2D models were used for further analysis. Based on the calibrated model results, bed friction and shoaling die out each other which wave height remain constant between PG1 and PG2 in the absence of PO leaves. Therefore, measured significant wave height can be considered net dissipation by the PO leaves only. A custom made 1D model also developed with the Dalrymple et.al (1983) formula to investigate the period or frequency dependent dissipation. 1D overestimates the dissipation with the same parameters used in 2D but it agrees with the measurement that waves at peak period dissipates more. On the other hand, in 1D model dissipates all the wave with periods greater than seven seconds while in measurement waves with large period does not affect from the PO leaves. There may be several scenarios for reasons of those results. One of them is related with the phase of the water particle motion and PO leave cluster can be inline which results minimal relative velocity and therefore less dissipation. Second scenario might be increase of velocity might break down the cluster structure of PO leaves which water particle does not feel the friction.

Third scenario might be the relative length of the test field with respect to wave length. Since in our case almost one wave length was passing through the test zone this may not be sufficient for a measurable dissipation. As we measured that lowest dissipation observed at 1.3 wave length in test zone there is possibility that in high wave period waves dissipation measured very less or zero.

Dimensionless comparison done with dimensionless period, T' and K_t. T is calculated by dividing each wave period to peak period. Results indicate that maximum dissipation occurs at rage of T' 0.9-1.1 without any dependence on the variation of PO leaves in the system which indicates periods close to peak period decay more than the others. We can conclude from this outcome that waves with the higher amplitude decays more than others. These findings are in agreement with Dalrymple *et al.* (1983) formula as dissipation has cubic relation with the horizontal velocity and velocity is linearly correlated with the wave amplitude. At lower and higher bounds of T, dissipation becomes dependent to PO leave concentration but in the lower bound dependence is more significant.

Another important dimensionless analysis is done with the relative field length where PO field length is normalized with the wave length (X'). In this analysis maximum dissipation is observed at X'= 1.17 i.e., where the PO zone length is 1.17 time greater than the wave length. In this band all of the waves dissipated more than 30% and up to 50 % dissipation observed. In overall most of the dissipation realized for the X' values between 1.08 to 1.31. On the other hand, it is noted that there is no significant dissipation observed at X'=1.05. These finding suggests that there is a strong relation for any dissipative medium with respect to wave length and dimension of the medium. For instance, wave energy harvesting systems or floating breakwaters are kind of wave dissipating systems. Findings here may be used or checked with similar systems which is left for future works.

At final stage an empirical formulation was derived based on the measured and calculated data. Formulation is dependent on the X' and α which is the PO concentration parameter.

Based on the promising outcome of this research regarding the wave dissipation capacity of PO leaves in their natural environment, it is recommended to local authorities to prohibit disposal of washed ashore PO leaves from the beaches and promote the use of PO as a nature-based solution to combat beach erosion around the world. As nature-based solution against erosion there is an understanding that it is not recommended to hydrodynamically energetic environments due to sensitivity of the plants against hydrodynamic forces. Considering the dead leaves capacity of wave dissipation, those plants can be transplanted in deeper sections of the energetic beaches where plants will not be affected from the wave forces, but in the period of defloration, they may serve as a protection measure as they will be transported to the nearshore.

7.2. Future Works

The defoliation of PO meadows in the Mediterranean Sea commences in autumn and followed by winter storms which pushes the leaves ashore. This migration of free-floating dead PO leaves continues throughout the autumn and winter months giving the PO leaves a prolonged duration of several months to spend in the nearshore zone. In case of beaches open to waves, washed ashore leaves may return to the sea and continue to contribute to wave dissipation in cycles. Therefore, to understand the overall dissipation capacity, it is vital to investigate the transport and fate mechanism of fallen the PO leaves. This subject may be linked with sediment transportation or sediment trapping capacity of the leaves.

Another important unknown is the behaviour of PO leaves in the breaking and swash zone. As shown in Figure 1.3. leaves are separated from the cluster while wave breaking and it is expected that considerable amount of energy is dissipated by the leaves which may prevent sediment resuspension. Figure 1.3. itself is self-explanatory how the PO leaves dissipates the wave energy in nearshore.

Important limitation to this study is that due to operational reasons with a limited band of PO concentration data is available and analysis is relied on this data. More controlled field test scheme is suggested to identify the dependence of the dissipation on PO concentration.

REFERENCES

1. UN Environment Programme, 2024, "UN Environment Programme", https://www. unep. org/ topics/ ocean- seas- and-coasts/ blue- ecosystems, accessed on June 09, 2024.

2. Inman, D.L. and R.A. Bagnold, Littoral Processes, in M.N. Hill, (ed.), "The Earth Beneath the Sea", New York, *John Wiley and Sons*, Vol. 1, No. 1, pp. 529-553, 1963.

3. Dean, R.G. and R.A., *Dalrymple, Coastal Processes with Engineering Applications*, Cambridge University Press, 2004.

4. Yılmaz, N., Balas, L. and A. İnan, "Coastal Erosion Problem, Modelling and Protection", *Ocean Science Journal*, Vol. 50, No. 1, 589-601, 2015.

5. Yüksek, Ö., H. Önsoy, A.R. Birben and I.H. Özölçer, "Coastal Erosion in Eastern Black Sea Region, Turkey", *Coastal Engineering*, Vol. 26, No. 3-4, pp. 225-239. 1995.

6. Google Earth Pro Version 7.3.6.9796, 2024, "Zone" 36 S 393720.83 M E 4050678.79 M N, Eye Altitude 4.1km, https:// www. researchgate. net/ figure/ UTM- zones- for- Turkey- fig1- 357579093, accessed on May 15, 2024.

7. Boudourresque C.F., G. Bernard, P. Bonhomme, E. Charbonnel, G. Diviacco, A. Meinesz, G. Pergent, C. Pergent-Martini, S. Ruitton, L. Tunesi, "Protection and Conservation of Posidonia Oceanica Meadows", *RAMOGE and RAC/SPA Publisher*, Tunis, Vol. 1, No. 1, pp. 1-202, 2012

8. Folkard, A.M., "Hydrodynamics of Model Posidonia Oceanica Patches in Shallow Wateri Limnology and Oceanography", *Wiley*, Vol. 50, No. 5, pp. 1592-1600, 2005.

9. Turna, İ.İ., Ü. Atik and U.G. Yıldırım, "Seasonal Variations of Posidonia Oceanica (L.) Delile in the Coasts of Alanya. Süleyman Demirel University", *Eğirdir Fisheries Faculty Journal*, Vol. 13, No. 1, pp. 1-11, 2017.

10. Mediterranean Wetland Initiative, "Available Online", https:// medwet. org/ 2017/ 10/ mediterranean- posidonia/, accessed on 19 January, 2023.

11. Lavery, P.S., M.Á. Mateo, O. Serrano and M. Rozaimi, "Variability Inass Habitats and its Implications for Global Estimates of Blue Carbon Ecosystem Service", *Plos One*, Vol. 8 No. 9, pp. 73748, 2013.

12. Drew, E.A. and B.P. Jupp, "Some aspects of the growth of Posidonia oceanica in Malta", *Underwater Research*, Vol. 1, No. 1, pp. 357-367. 1976.

13. Price, W A., K.W. Tomlinson and J.N. Hunt, "The Effect of Artificial Seaweed in Promoting the Build-Up of Beaches", *In Coastal Engineering*, Vol. 1, No. 1, pp. 570-578, 1968.

14. Chastel, T., K. Botten, N. Durand and N. Goutal, "Bulk Drag Coefficient of a Subaquatic Vegetation Subjected to Irregular Waves: Influence of Reynolds and Keulegan-Carpenter Numbers", *La Houille Blanche*, Vol. 106, No. 2, pp. 34-42, 2020.

15. Dalrymple, R.A., J.T. Kirby, and P.A. Hwang, "Wave Diffraction Due to Areas of Energy Dissipation, Journal of Waterway, Port", *Coastal, and Ocean Engineering*, Vol. 110, No. 1, pp. 67-79, 1984.

16. Kobayashi, N., A.W. Raichle and T. Asano, "Wave Attenuation by Vegetation", *Journal of Waterway, Port, Coastal, and Ocean Engineering*, Vol. 119, No. 1, pp. 30-48, 1993.

17. Mendez, F J. and I.J. Losada, "An Empirical Model to Estimate the Propagation of Random Breaking and Nonbreaking Waves Over Vegetation Fields", *Coastal*

Engineering, Vol. 51, No. 2, pp. 103-118, 2004.

18. Koftis, T., P. Prinos and V. Stratigaki, "Wave Damping Over Artificial Posidonia Oceanica Meadow, a Large-Scale Experimental Study", *Coastal Engineering*, Vol. 73, No. 1, pp. 71-83, 2013.

19. Hu, Z., T. Suzuki, T. Zitman, W. Uittewaal and M. Stive, "Laboratory Study on Wave Dissipation by Vegetation in Combined Current–Wave Flow", *Coastal Engineering*, Vol. 88, No. 1, pp. 131-142, 2014.

20. Bradley, K. and C. Houser, "Relative Velocity of Seagrass Blades: Implications for Wave Attenuation in Low-Energy Environments", *Journal of Geophysical Research*, Vol. 114, No. 1, pp. F01004-F01024, 2009.

21. Peruzzo, P., F. De Serio, A. Defina, and M. MossaWave, "Height Attenuation and Flow Resistance Due to Emergent or Near-Emergent Vegetation", *Water*, Vol. 10, No. 4, pp. 402, 2018.

22. Luhar, M., E. Infantes and H. Nepf, "Seagrass Blade Motion Under Waves and its Impact on Wave Decay", *Journal of Geophysical Research, Oceans*, Vol. 122, No. 5, pp. 3736-3752, 2017.

23. 23. Chastel, T., K. Botten, N. Durand and N. Goutal, "Bulk Drag Coefficient of a Subaquatic Vegetation Subjected to Irregular Waves, Influence of Reynolds and Keulegan-Carpenter Numbers", *La Houille Blanche*, Vol. 106, No. 2, pp. 34-42, 2020.

24. Henry, P.Y., D. Myrhaug and J. Aberle, "Drag Forces on Aquatic Plants in Non-linear Random Waves Plus Current, Estuarine", *Coastal and Shelf Science*, Vol. 165, No. 1, pp. 10-24, 2015.

25. John, B.M., K.G. Shirlal and S. Rao, "Effect of Artificial Sea Grass on Wave Attenuation-An Experimental Investigation", *Aquatic Procedia*, Vol. 4, No. 1, pp.

221-226, 2015.

26. Augustin, L.N., J.L. Irish and P. Lynett, "Laboratory and Numerical Studies of Wave Damping by Emergent and Near-Emergent Wetland Vegetation", *Coastal Engineering*, Vol. 56, No. 3, pp. 332-340, 2009.

27. Astudillo, C., V. Gracia, I. Cáceres, J.P. Sierra and A. Sánchez-Arcilla, "Beach Profile Changes Induced by Surrogate Posidonia Oceanica, Laboratory Experiments", *Coastal Engineering*, Vol. 175, No.1, pp. 104144, 2022.

28. Fonseca, M.S. and J.A. Cahalan, "A Preliminary Evaluation of Wave Attenuation by Four Species of Seagrass, Estuarine", *Coastal and Shelf Science*, Vol. 35, No. 6, pp. 565-576, 1992.

29. Hendriks, I.E., T. Sintes, T.J. Bouma and C.M. Duarte, "Experimental Assessment and Modeling Evaluation of the Effects of the Seagrass Posidonia Oceanica on Flow and Particle Trapping", *Marine Ecology Progress Series*, Vol. 356, No. 1, pp. 163-173, 2008.

30. Manca, E., I.J. Cáceres, I. V, J.M. Alsina, V. Stratigaki, I. Townend and C.L. Amos, "Wave Energy and Wave-Induced Flow Reduction by Full-Scale Model Posidonia Oceanica Seagrass", *Continental Shelf Research*, Vol. 50, No. 1, pp. 100-116, 2012.

31. 31. Elginoz, N., M.S. Kabdasli and A. Tanik, "Effects of Posidonia Oceanica Seagrass Meadows on Storm Waves", *Journal of Coastal Research*, Vol. 1, No. 1, pp. 373-377, 2011.

32. Zhang, X., P. Lin, Z. Gong, B. Li and X. Chen, "Wave Attenuation by Spartina Alterniflora Under Macro-Tidal and Storm Surge Conditions", *Wetlands*, Vol. 40, No. 1, pp. 2151-2162, 2020.

33. Zhu, Q., P.L. Wiberg and K.J. McGlathery, "Seasonal Growth and Senescence

of Seagrass Alters Sediment Accumulation Rates and Carbon Burial in a Coastal Lagoon", *Limnology and Oceanography*, Vol. 67, No.9, pp. 1931-1942, 2022.

34. Higgins, L., "On the Statistical Distribution of the Heights of Sea Waves", *Journal of Marine Research*, Vol.11, No. 3, pp. 245-266, 1952.

35. Vatankhah, A.R. and Z. Aghashariatmadari, "Improved Explicit Approximation of Linear Dispersion Relationship for Gravity Waves", *Comment on Another Discussion, Coastal Engineering*, Vol. 81, No. 1, pp. 30-31, 2013.

36. Swan Scientific and Technical Documentation, *Swan Cycle III version 41.45AB*, The Swan Team, Delft, 19 March 2024.

37. Hasselmann, K., T.P. Barnett, E. Bouws, H. Carlson, D.E. Cartwright, K. Enke and H. Walden, *Measurements of Wind-Wave Growth and Swell Decay During the Joint North Sea Wave Project (JONSWAP)*, Ergaenzungsheft Zur Deutschen Hydrographischen Zeitschrift, Reihe A., 1973.

38. Mendez, F.J., I.J. Losada, R.A. Dalrymple and M.A. Losada, "Effects of Wave Reflection and Dissipation on Wave-Induced Second Order Magnitudes", *In Coastal Engineering*, Vol. 1, No. 1, pp. 537-550, 1998.

39. Yüksel, Y., E. Çevik, B. Aydoğan, A. Arı, K.E. Saraçoğlu, R. Alpli and B. Bekar, "Wave Climate Model of the Turkish Seas and Long-Term Wave Climate Analysis", *7th National Coastal Engineering Symposium*, Vol. 1, No. 1, pp. 411-420, 2011.

40. Nowacki, D.J., A. Beudin and N.K. Ganju, "Spectral Wave Dissipation by Submerged Aquatic Vegetation in a Back-Barrier Estuary", *Limnology and Oceanography*, Vol. 62, No. 2, pp. 736-753, 2017.

41. Zhu, L., J. Lei, K. Huguenard and D.W. Fredriksson, "Wave Attenuation by Suspended Canopies with Cultivated Kelp" (Saccharina Latissima), *Coastal Engineering*, Vol. 168, No. 1, pp. 103947, 2021.

APPENDIX A: ENERGY SPECTRUM FOR BURST 3-13

The energy spectra of waves for Bursts 3 to 13 are shown in Figure A.1 to Figure A.11 below. The first two waves (Bursts 1 and 2) and the last two waves (Bursts 14 and 15) are presented in Figure 6.1

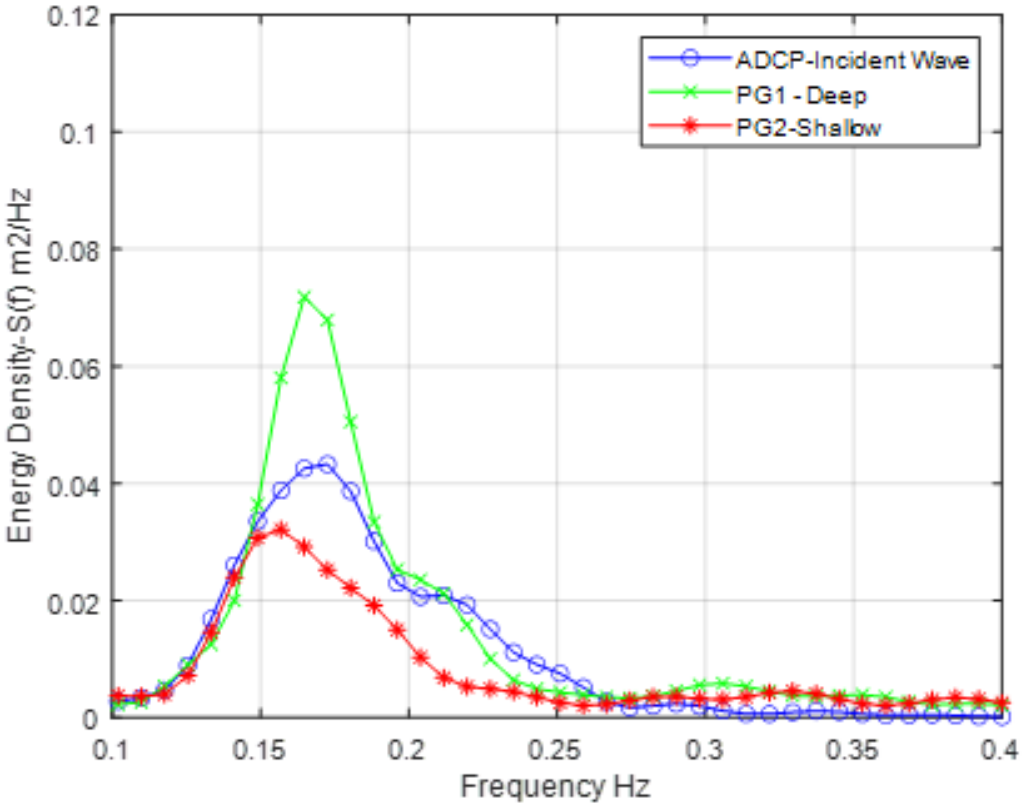

Figure A.1. Energy spectrum for wave burst 3.

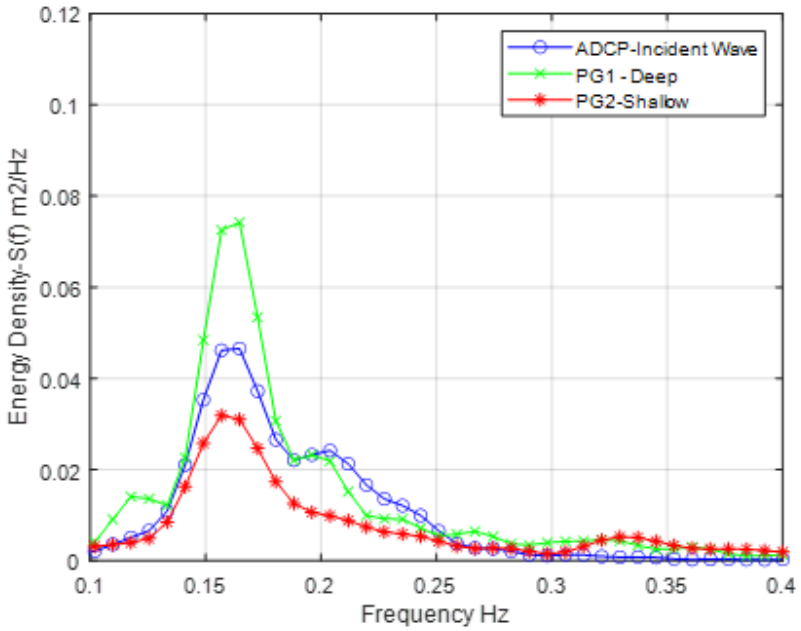

Figure A.2. Energy spectrum for wave burst 4.

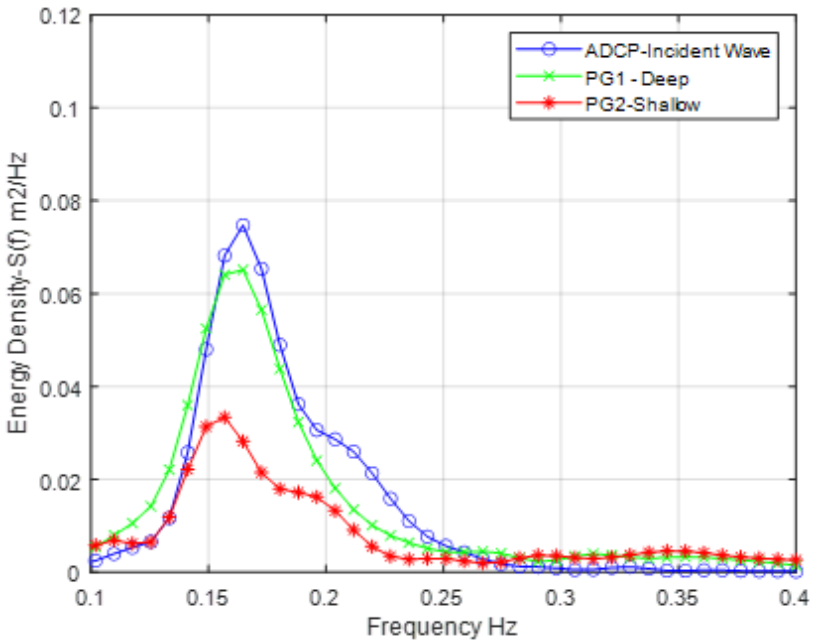

Figure A.3. Energy spectrum for wave burst 5.

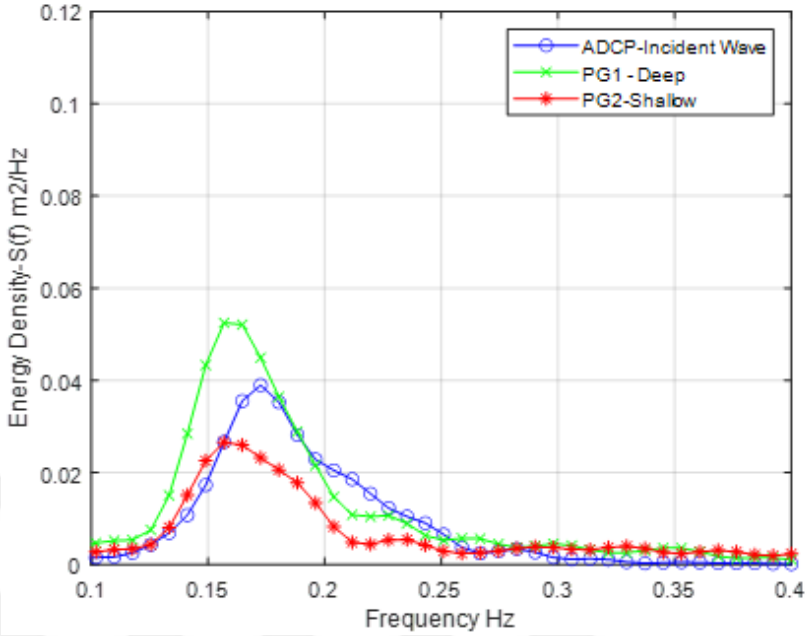

Figure A.4. Energy spectrum for wave burst 6.

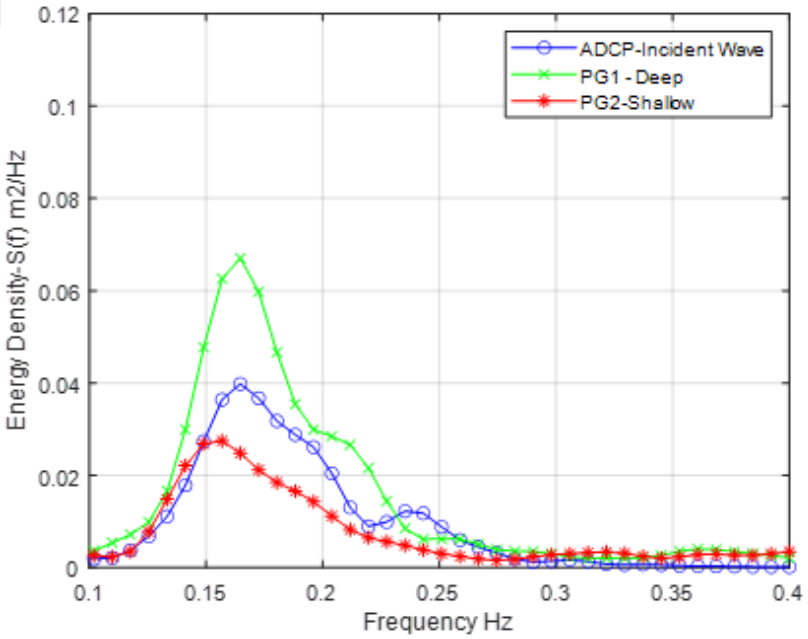

Figure A.5. Energy spectrum for wave burst 7.

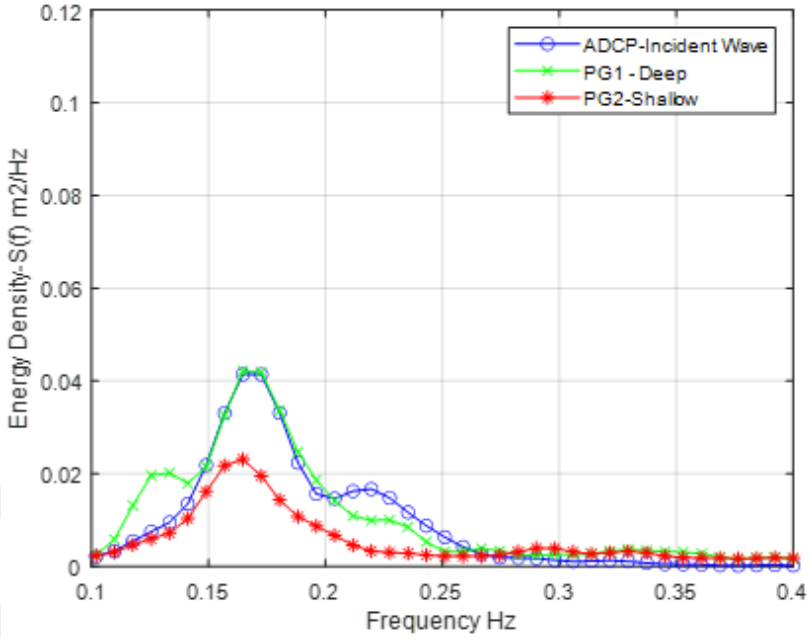

Figure A.6. Energy spectrum for wave burst 8.

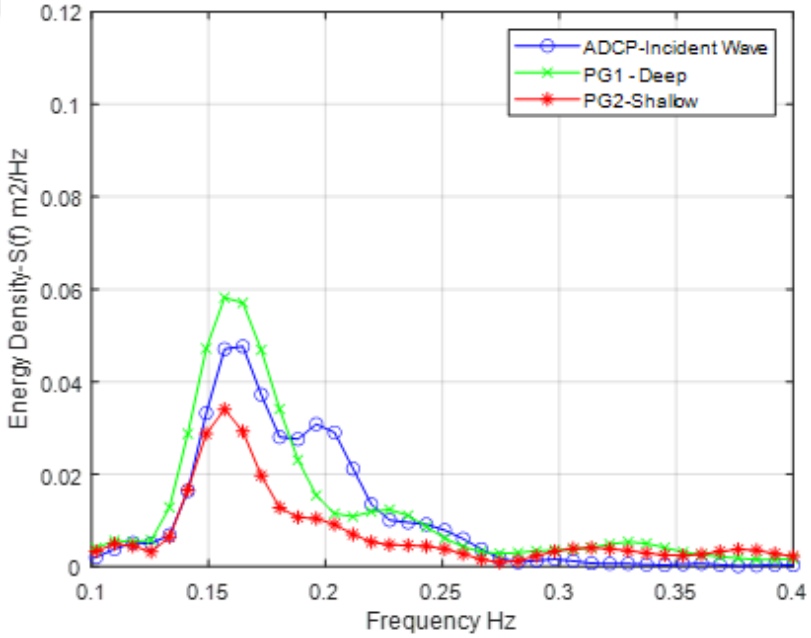

Figure A.7. Energy spectrum for wave burst 9.

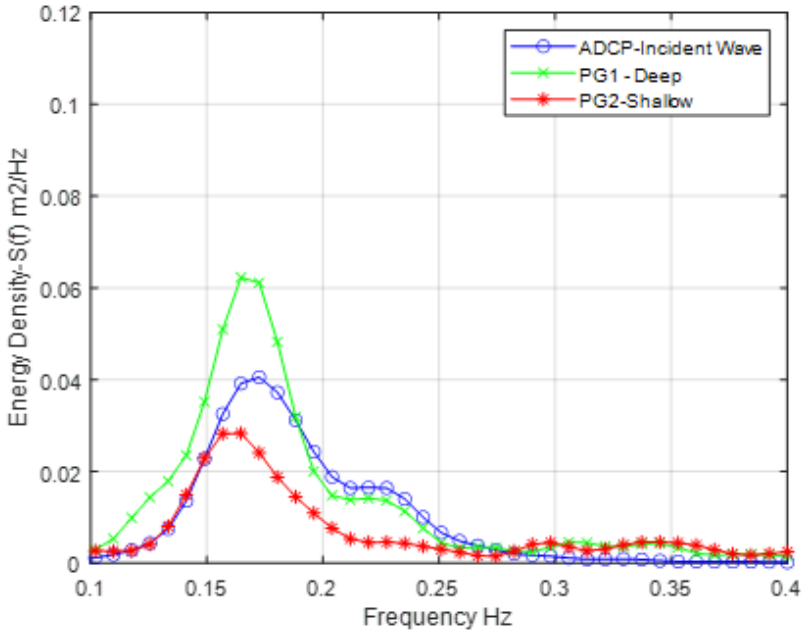

Figure A.8. Energy spectrum for wave burst 10.

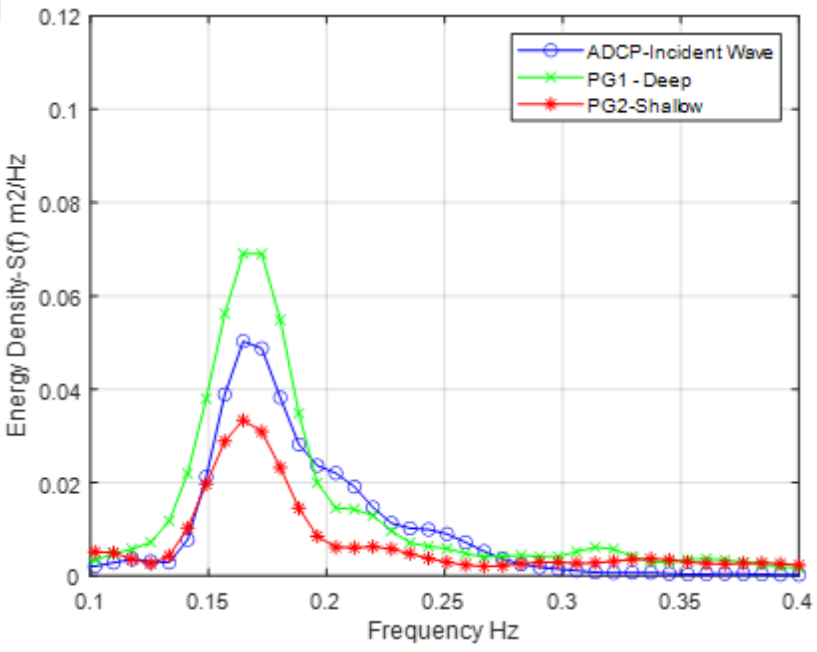

Figure A.9. Energy spectrum for wave burst 11.

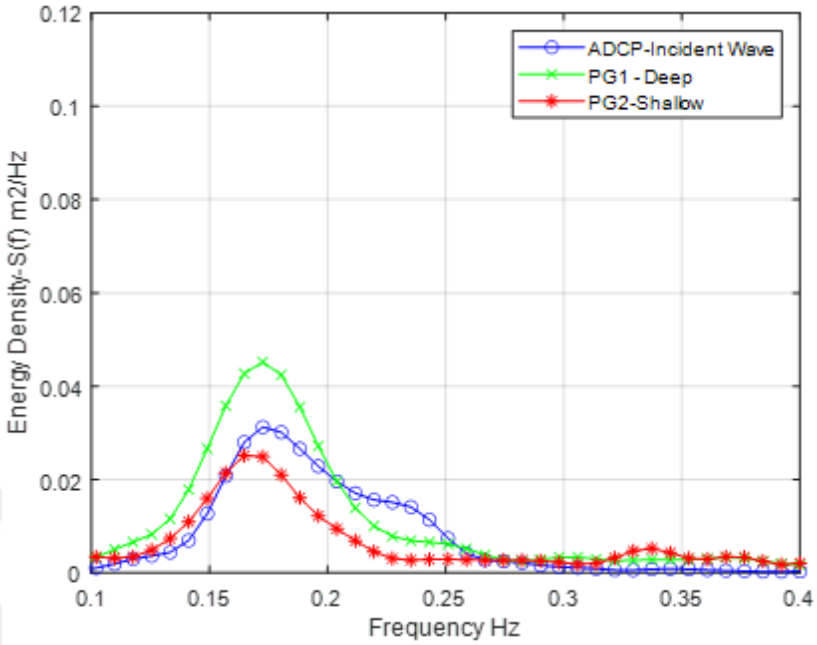

Figure A.10. Energy spectrum for wave burst 12.

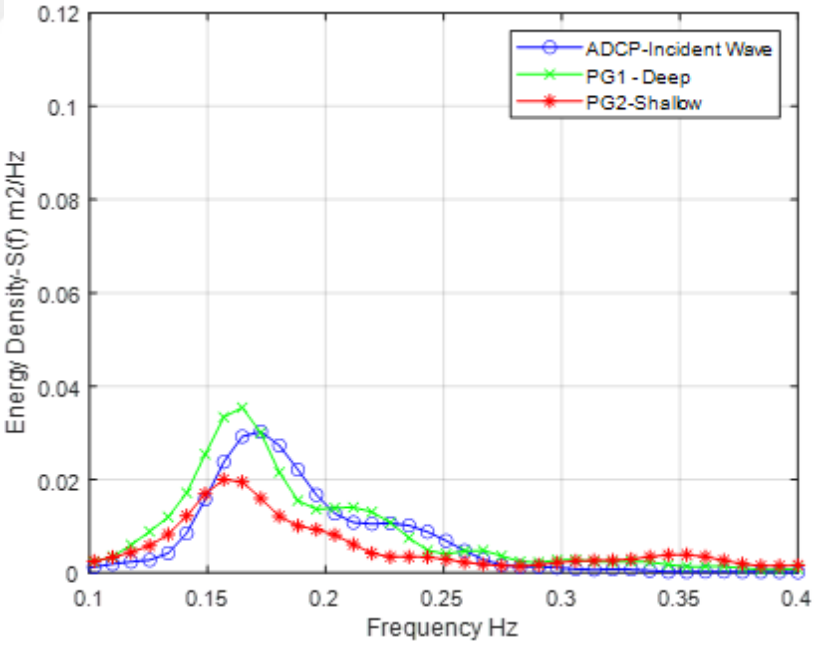

Figure A.11. Energy spectrum for wave burst 13.

APPENDIX B: 2D MODEL CONTOUR OUTPUTS FOR BURSTS 2-14

The 2D model output and contour view of the measurement field for Bursts 2 and 14 are shown in Figure B.1 to Figure B.4 below. The contour view and model output for Bursts 1 and 2 are presented in Figure 6.11 and Figure 6.12, respectively.

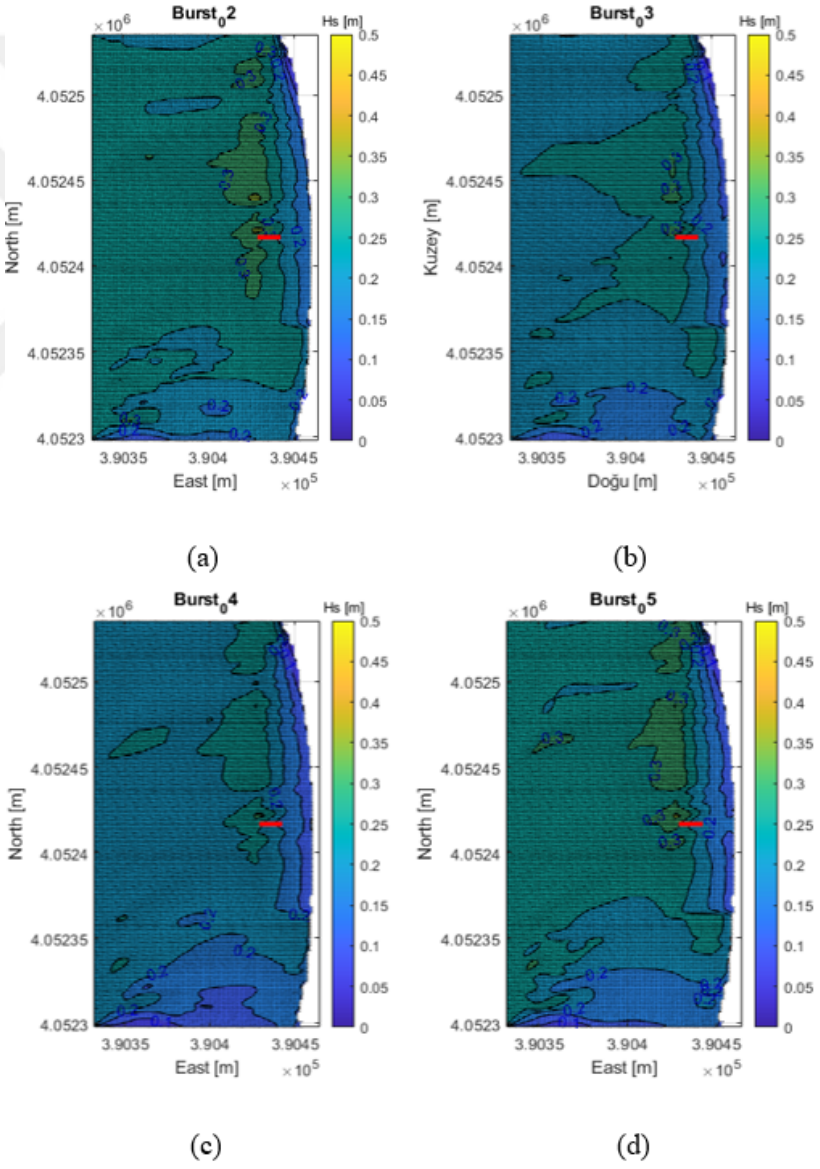

Figure B.1. 2D Model contour output for bursts (a) 2 (b) 3 (c) 4 (d) 5.

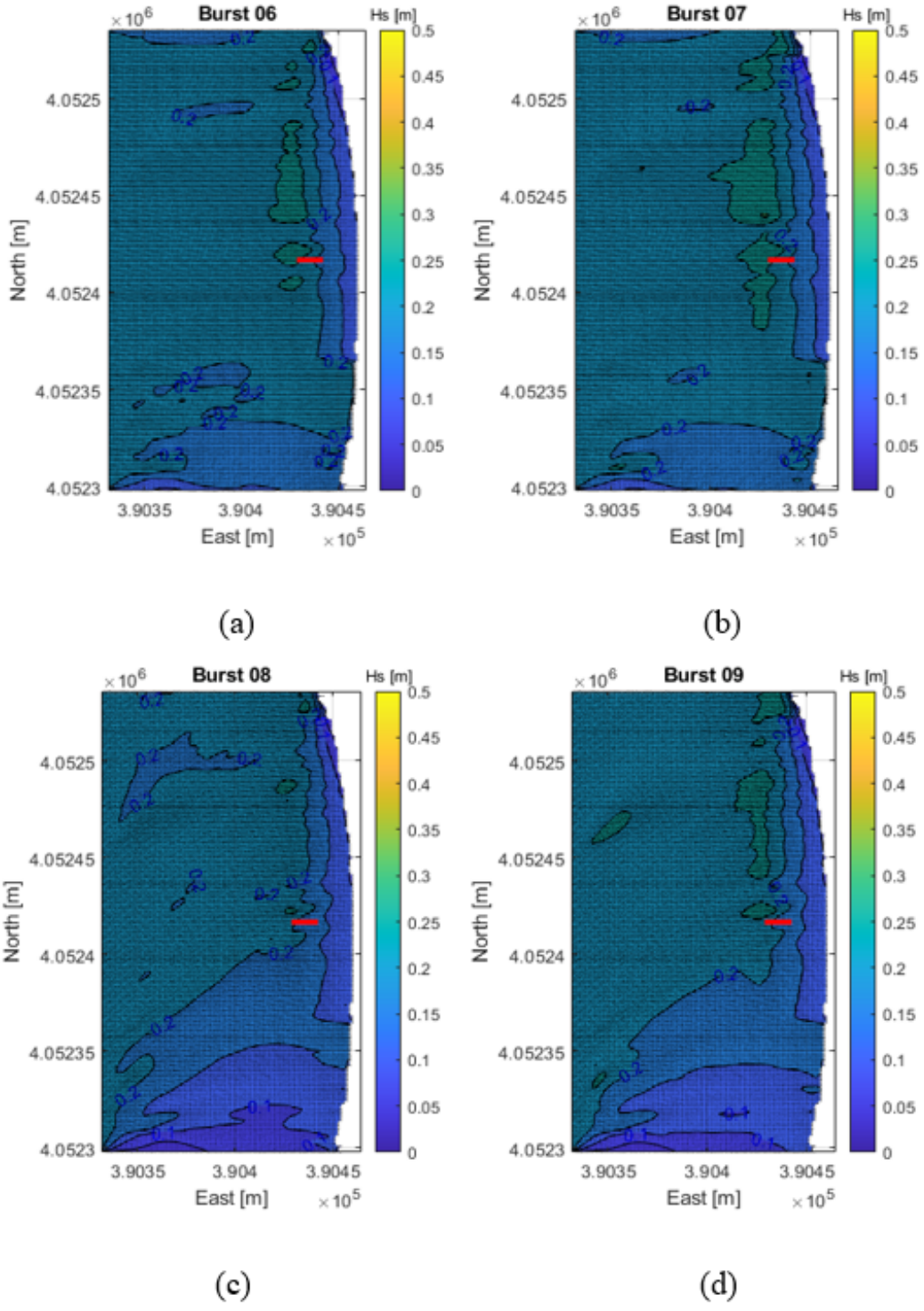

Figure B.2. 2D Model contour output for bursts (a) 6 (b) 7 (c) 8 (d) 9.

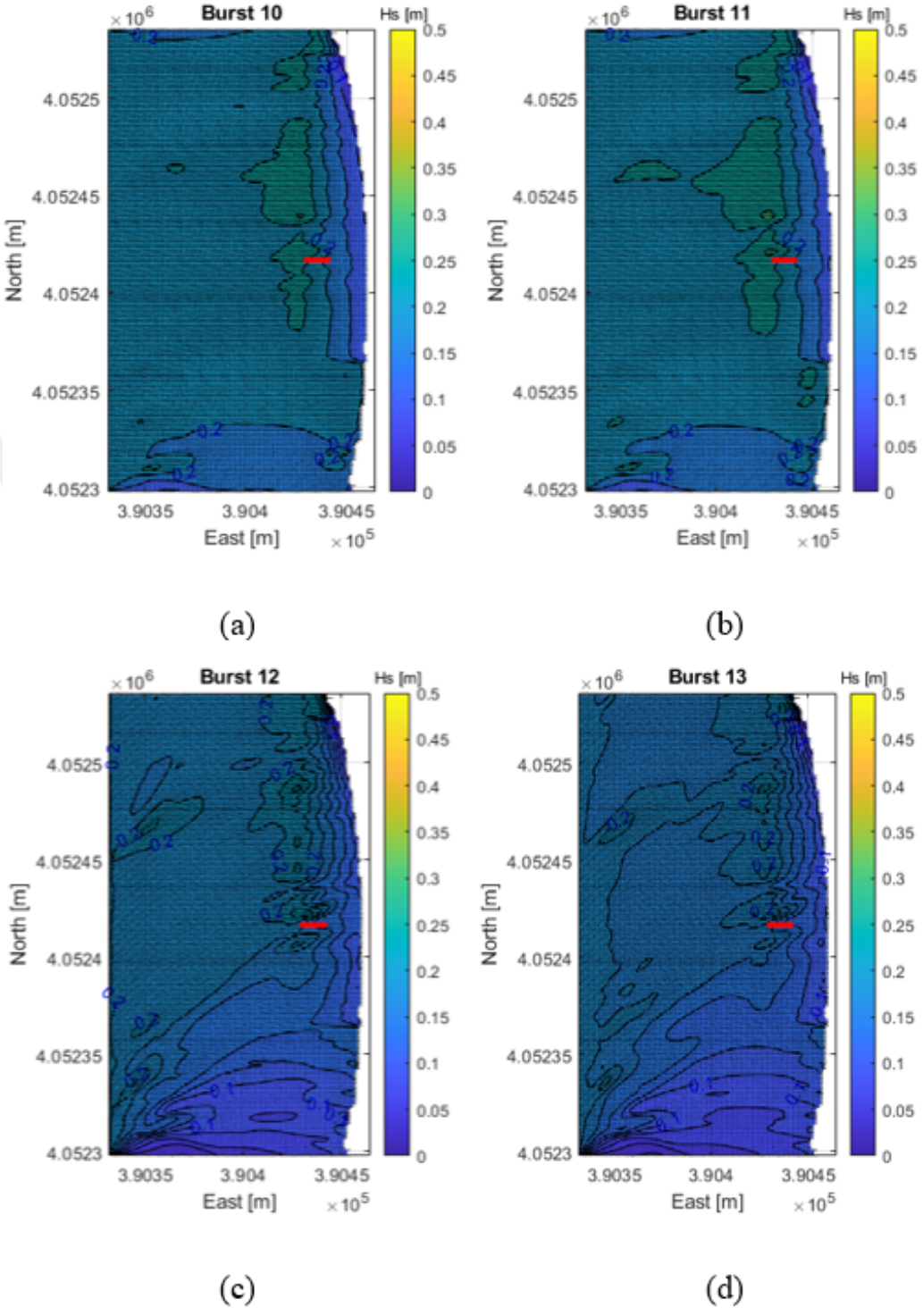

Figure B.3. 2D Model contour output for bursts (a) 10 (b) 11 (c) 12 (d) 13.

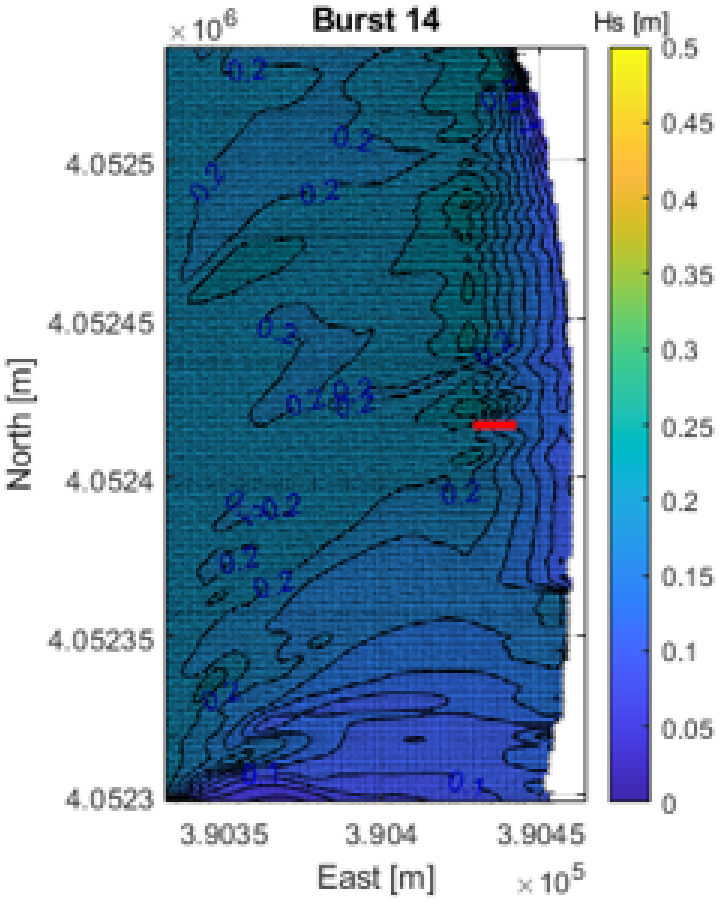

Figure B.4. 2D Model contour output for bursts 14.